MEASUREMENTS OF DYNAMIC PROPERTIES OF MATERIALS

Volume VI

TANTALUM

FINAL REPORT

by

W. M. Isbell
D. R. Christman
S. G. Babcock

Materials and Structures Laboratory
Manufacturing Development, General Motors Corporation
General Motors Technical Center, Warren, Michigan 48090

Destroy this report when it is no longer needed Do not return to sender

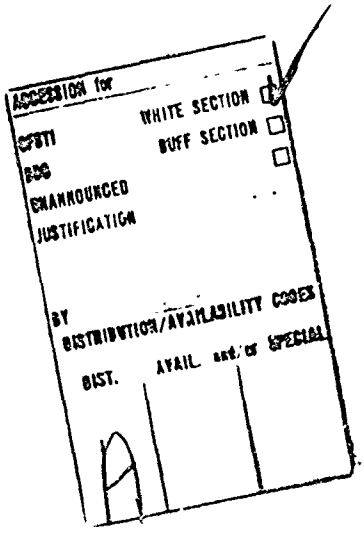

UNCLASSIFIED
Security Classification

DOCUMENT CONTROL DATA - R & D

(Security classification of title, body of abstract and indexing annotation must be entered when the overall report is classified)

1. ORIGINATING ACTIVITY (Corporate author): Manufacturing Development, General Motors Corporation, General Motors Technical Center, Warren, Michigan 48090

2a. REPORT SECURITY CLASSIFICATION: UNCLASSIFIED

2b. GROUP:

3. REPORT TITLE

Measurements of Dynamic Properties of Materials Volume VI: Tantalum

4. DESCRIPTIVE NOTES (Type of report and inclusive dates)

Final Report (in Six Volumes)

5. AUTHOR(S) (First name, middle initial, last name)

William M. Isbell, Douglas R. Christman, Stephen G. Babcock

6. REPORT DATE	7a. TOTAL NO. OF PAGES	7b. NO. OF REFS
1971 November	88	54

8a. CONTRACT OR GRANT NO.	9a. ORIGINATOR'S REPORT NUMBER(S)
DASA01-68-C-0114	
b. PROJECT NO. NEWR XAXA	MSL-70-23, Vol. VI
c. Task and Subtask A106	9b. OTHER REPORT NO(S) (Any other numbers that may be assigned this report)
d. Work Unit 07	DASA 2501-6

10. DISTRIBUTION STATEMENT

Approved for public release; distribution unlimited.

11. SUPPLEMENTARY NOTES	12. SPONSORING MILITARY ACTIVITY
	Director Defense Nuclear Agency Washington, D. C. 20305

13. ABSTRACT

Results of an experimental study on the dynamic properties of tantalum are presented. Areas studied included stress-strain-strain rate and reverse loading behavior, elastic constants, equation of state, compressive and release wave characteristics, and spall fracture. The material showed approximately elastic-plastic behavior with some strain hardening under uniaxial stress compression, and exhibited strain-rate sensitivity with yield under uniaxial stress increasing from 1.4 to ∿ 5.4 kbar for a strain rate increase of 0.001 to 800/sec. Longitudinal and shear wave velocities at 20°C were 4.146 and 2.032 mm/μsec, and temperature and pressure dependence was also measured and various elastic constants were calculated. The shock wave equation of state (EOS) up to 200 kbar was determined as $\sigma_H = 4.0 + 550\ u_p + 215\ u_p^2$. The EOS was also calculated from the elastic constants and comparisons made with the shock wave EOS. Compressive wave tests showed a well-defined elastic precursor with a steady-state value of 15 kbar. The impact velocity required for spall fracture was found to increase with decreasing pulse width.

DD FORM 1 NOV 35 1473

UNCLASSIFIED
Security Classification

14. KEY WORDS	LINK A		LINK B		LINK C	
	ROLE	WT	ROLE	WT	ROLE	WT
Stress-strain-strain rate Reverse loading behavior Elastic constants Equation of State Compressive and release wave characteristics Spall fracture						

DASA 2501-6
MSL-70-23 Vol. VI
1972, February

MEASUREMENTS OF DYNAMIC PROPERTIES OF MATERIALS

Volume VI

TANTALUM

FINAL REPORT

" This work was supported by the Defense Nuclear Agency under NWER Subtask AA 106-07"

by

W. M. Isbell*
D. R. Christman
S. G. Babcock

Materials and Structures Laboratory
Manufacturing Development, General Motors Corporation
General Motors Technical Center, Warren, Michigan 48090

* Presently with the University of California, Lawrence Livermore Laboratory, Livermore, California.

Prepared For

HEADQUARTERS
Defense Nuclear Agency
Washington, D.C. 20305

Under Contract DASA01-68-C-0114

COPY No. 1

MSL-70-23, Vol. VI

ABSTRACT

Results of an experimental study on the dynamic properties of tantalum are presented. Areas studied included stress-strain-strain rate and reverse loading behavior, elastic constants, equation of state, compressive and release wave characteristics, and spall fracture. The material showed approximately elastic-plastic behavior with some strain hardening under uniaxial stress compression, and exhibited strain-rate sensitivity with yield under uniaxial stress increasing from 1.4 to ∿ 5.4 kbar for a strain rate increase of 0.001 to 800/sec. Longitudinal and shear wave velocities at 20°C were 4.146 and 2.032 mm/μsec, and temperature and pressure dependence was also measured and various elastic constants were calculated. The shock wave equation of state (EOS) up to 200 kbar was determined as $\sigma_H = 4.0 + 550\ u_p + 215\ u_p^2$. The EOS was also calculated from the elastic constants and comparisons made with the shock wave EOS. Compressive wave tests showed a well-defined elastic precursor with a steady-state value of ∿ 15 kbar. The impact velocity required for spall fracture was found to increase with decreasing pulse width.

FOREWORD

The prediction of reentry vehicle response to impulsive loading resulting from energy deposition has been studied extensively during the last decade. Analytical models and computer routines have been developed to assess the vulnerability of such vehicles to the initial loading phase, in which stress waves are generated and propagated through the structure, and to subsequent phases, where elastic vibration, plastic deformation and/or fracture may occur.

A Defense Nuclear Agency (DNA) program was initiated with the objective of improving computer codes for the prediction of damage induced by X-rays (PREDIX). The PREDIX metals program has combined the efforts of several contractors under the direction of DNA. The primary contributions of each contractor can be summarized as follows:

General Motors Corporation--Measurement of material properties, including stress-strain-strain rate behavior, elastic constants, equations of state, shock wave profiles and spall fracture.

Effects Technology Inc.--Spall fracture tests and analysis (exploding foil) and underground testing.

KMS Technology Center--Constitutive modeling.

Physics International Company--Energy deposition and spall fracture studies (electron beam).

Systems, Science and Software--Energy deposition and front surface phenomena, constitutive modeling and code development, and underground testing.

TABLE OF CONTENTS

TABLE OF CONTENTS (Continued)

LIST OF ILLUSTRATIONS

LIST OF ILLUSTRATIONS (Continued)

LIST OF TABLES

LIST OF SYMBOLS

C_B	Bulk Wave Velocity, mm/μsec
C_L	Longitudinal Wave Velocity, mm/μsec
C_S	Shear Wave Velocity, mm/μsec
c_p	Specific Heat, cal/g
G	Shear Modulus, kbar
K	Bulk Modulus, kbar
P_H	Mean Pressure, Hydrostat, kbar
P_S	Mean Pressure, Adiabat, kbar
P_T	Mean Pressure, Isotherm, kbar
T	Temperature, °C
U_S	Shock Wave Velocity, mm/μsec
u_p	Particle Velocity, mm/μsec
v	Specific Volume, cc/g
V_I	Impact Velocity, mm/μsec
X	Target Thickness, mm
X_O	Impactor Thickness, mm
X^S	Adiabatic Modulus, kbar
X^T	Isothermal Modulus, kbar
$X^{S'}_{OS}$, $X^{T'}_{OS}$	Adiabatic Pressure Derivative @ Zero Pressure $\left(= \left(\frac{\partial X^S}{\partial P}\right)_S \Big|_{P=0}\right)$
$X^{T'}_{OT}$, $X^{S'}_{OT}$	Isothermal Pressure Derivative @ Zero Pressure $\left(= \left(\frac{\partial X^T}{\partial P}\right)_T \Big|_{P=0}\right)$
β	Volume Coefficient of Expansion, /°C $= -\frac{1}{\rho}\left(\frac{\partial \rho}{\partial T}\right)_{P=0}$
γ	Gruneisen Parameter
μ	Compression $(= v_o/v - 1)$
ν	Poisson's Ratio
ρ	Density, g/cc
σ_H	Stress, Hugoniot, kbar

(Page x is Blank)

INTRODUCTION

This report is one of a series of six giving results of a study of dynamic properties of four metals. The principle objectives of this study were:

- Provide measurements of dynamic properties of materials to be used as inputs to model development for shock wave propagation and dynamic fracture.

- Provide data to establish accuracy of computer code predictions.

- Provide physical interpretation of experimentally observed material response to dynamic test conditions.

The primary areas studied included: (1) Stress-strain-strain rate behavior in uniaxial stress, including Bauschinger effect; (2) Elastic constants, including temperature and pressure dependence; (3) Hugoniot equation of state; (4) Compressive and release wave profiles, including elastic precursor decay and wave attenuation; and (5) Spall fracture studies, including pulse width dependence. The six reports in this series are:

Vol. I: Summary of Results, DASA 2501-1 (AD712847)
Vol. II: Experimental Methods and Techniques, DASA 2501-2 (AD 730750)
Vol. III: 6061-T6 Aluminum, DASA 2501-3
Vol. IV: Alpha Titanium, DASA 2501-4
Vol. V: OFHC Copper, DASA 2501-5 (AD 728846)
Vol. VI: Tantalum, DASA 2501-6

The experimental techniques utilized in this study are reviewed in Vol. II (DASA 2501-2). Briefly, the principal techniques applied were:

Stress-strain Studies--A laboratory-type universal testing machine was used for rates < 0.1/sec, a medium strain rate machine for rates of 10^{-3}/sec to 10^{2}/sec, and a Hopkinson bar device for rates of about 10^{2} to 5 X 10^{3}/sec.

Elastic Constants--The pulse superposition method was used for measuring longitudinal and shear wave velocities as functions of temperature and hydrostatic pressure.

Equation of State--Gun-launched, flat-plate impact techniques were used to generate uniaxial strain conditions. Velocities up to 0.6 mm/μsec were achieved with 63.5 mm and 102 mm single-stage compressed-gas guns. Hugoniot data were obtained with x-cut quartz gages.

Wave Propagation and Spall Fracture--Flat-plate impact techniques were also used. Wave profiles were measured with x-cut quartz gages and a laser velocity interferometer.

A literature search on dynamic properties of materials was carried out under the PREDIX program and a listing of recent publications (including abstracts) on dynamic properties of materials is given in Reference 1.

SECTION I

MATERIAL PROPERTIES

Tantalum has a body-centered-cubic structure and the material on which tests discussed in this report were carried out was a commercially pure grade of 99.5% purity. This material was purchased as 50.8 mm diameter bar stock, which was preferrable to plate or sheet stock since it provided specimens of various thicknesses and gave little scrap while ensuring that all specimens were from the same parent material. Chemical analysis performed by the supplier* gave:

Columbium	210 ppm
Tungsten	120
Iron	20
Carbon	<10
Oxygen	38
Nitrogen	22
Hydrogen	<5

Tantalum is not heat-treatable and different strength levels are achieved by slight changes in impurity content or by cold-working. Although not specified, the material apparently had been annealed. Certifications gave 1.8 kbar tensile yield

*Fansteel, Inc., Lot No. 69B-2522, 31 July 1969.

strength, 2.35 kbar ultimate tensile strength and 52% elongation at 4D (measured along the bar axis). Measured hardness was 52 R_K. A photomicrograph of a representative portion of the bar is shown in Figure 1. The bar axis or centerline is vertical and the width shown is ∿ 5 mm out of a total of 50.8 mm. There was a slight grain elongation along the axis and about a factor of 10 variation in grain size, ranging from ASTM 6 to 00 (45 to 500 μm). For results presented in this report, the test or wave propagation direction was axial (e.g., vertical in Figure 1).

The average measured density (ρ_o) was 16.66 g/cc (0.601 lb/in^3). For use in equation of state and energy deposition claculations, several physical constants were compiled from the literature[2-5] and are listed below:

Volume coefficient of thermal expansion, β:

$19.8 \times 10^{-6} + 0.001 \times 10^{-6}$ T/°C

Specific heat, c_p:

$0.034 + 10^{-5}$ T cal/g/°C

Melting temperature: 2996°C

Boiling temperature: 5430°C

Latent heat of fusion: 35 cal/g

Latent heat of vaporization: 1000 cal/g

(T in °C)

A portion of the tantalum bar was annealed for 1 hour at 1200°C in vacuum. The structure of this material is compared to the as-received material in Figure 2. There was no significant change in structure or hardness.

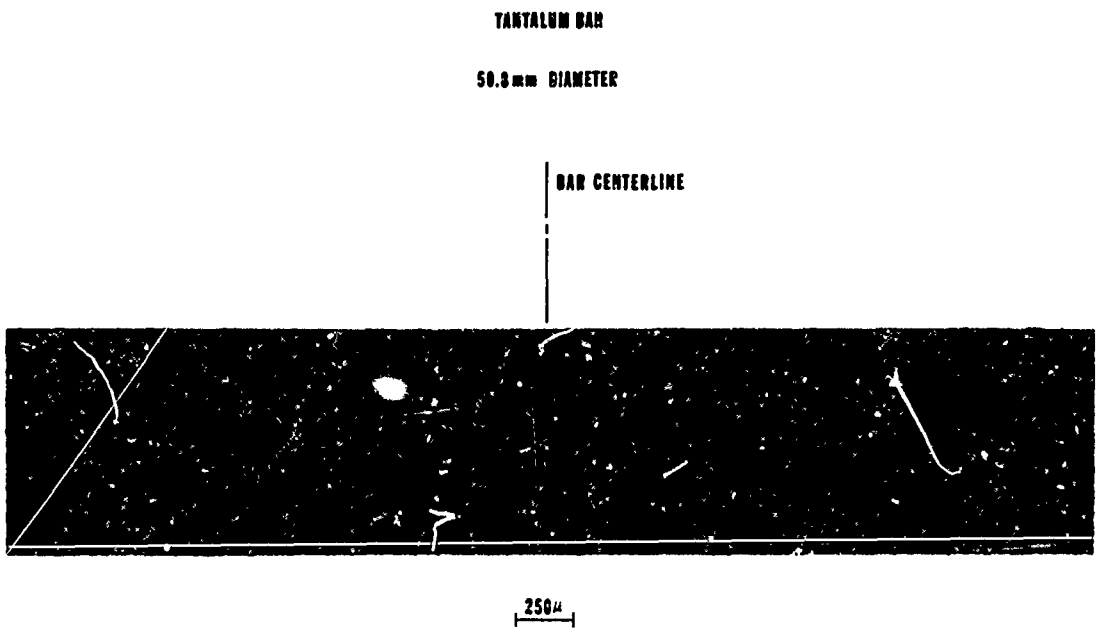

Figure 1 Tantalum Bar Stock, Grain Structure

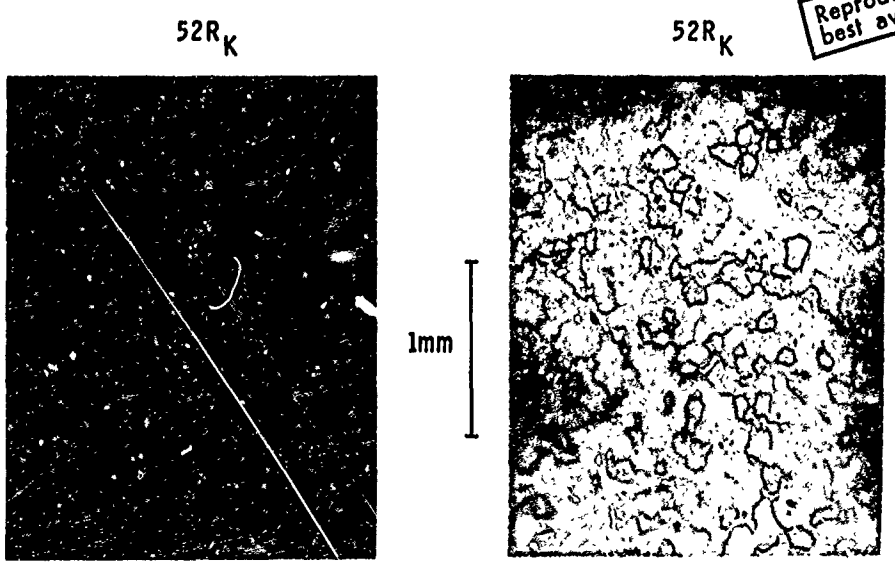

Figure 2 As-Received and Annealed Tantalum

SECTION II

STRESS-STRAIN STUDIES

Shock wave and structural response code input requirements include constitutive equations relating stress to strain and strain rate. Uniaxial stress tests at various strain rates give yield and flow stress behavior, strain rate sensitivity and work hardening characteristics. Bauschinger effect tests were conducted to provide data on unloading and subsequent yield behavior.

UNIAXIAL STRESS TESTS*

The compressive stress-strain-rate behavior of tantalum at 20°C is shown in Figure 3 for strain rates of 10^{-3}/sec to 600/sec, with each curve the average of three tests. The material is very strain-rate sensitive, showing an almost 300% increase in yield level over this range of strain rates. A slight yield drop is evident above a rate of 40/sec. Strain rate data are cross-plotted in Figure 4 to give true stress vs. log true strain rate. Both yield and flow stress (6% strain) increase with strain rate, with sensitivity (slope) becoming very high above 100/sec.

---

* Deformation mechanisms of tantalum (primarily under uniaxial stress conditions) have been studied by a number of other investigators. The reader is referred to the literature for details in such areas as strain rate effects (Refs. 6-10, temperature effects (8-14), impurity content (6, 13-16), stress relaxation (9,17) grain size effects (14, 17) dislocation behavior (11, 15-18), anisotropy (19), and fracture (12).

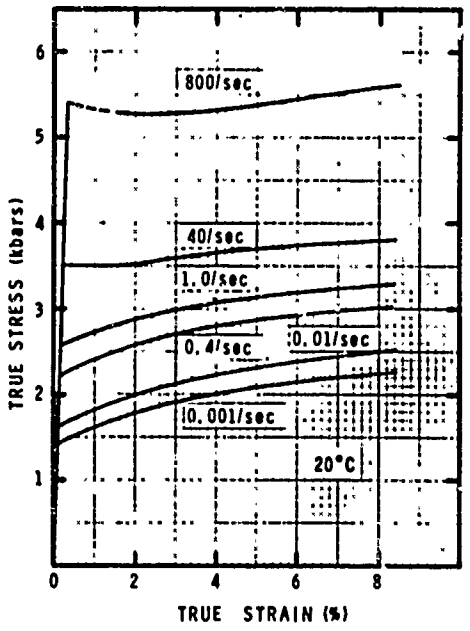

Figure 3 Compressive Stress vs. Strain, Tantalum

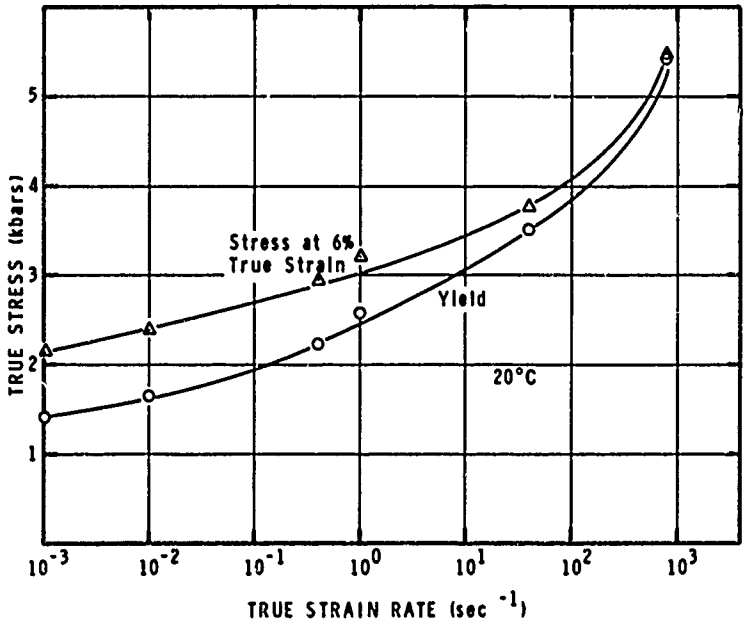

Figure 4 Compressive Stress vs. Log Strain Rate, Tantalum

REVERSE LOADING TESTS

The reverse loading behavior or Bauschinger effect was studied by performing uniaxial tension tests after the material had been prestrained in the opposite (compressive) direction. Results from low strain rate (0.001/sec) tests are given in Figure 5 for maximum strains of 0.5, 1, and 3%. The Bauschinger strain (defined here as the plastic strain in the reverse loading path at 3/4 of the initial yield stress) is insensitive to prestrain, at least up to 3% strain. Flow stress in tension has increased with increasing compressive prestrain.

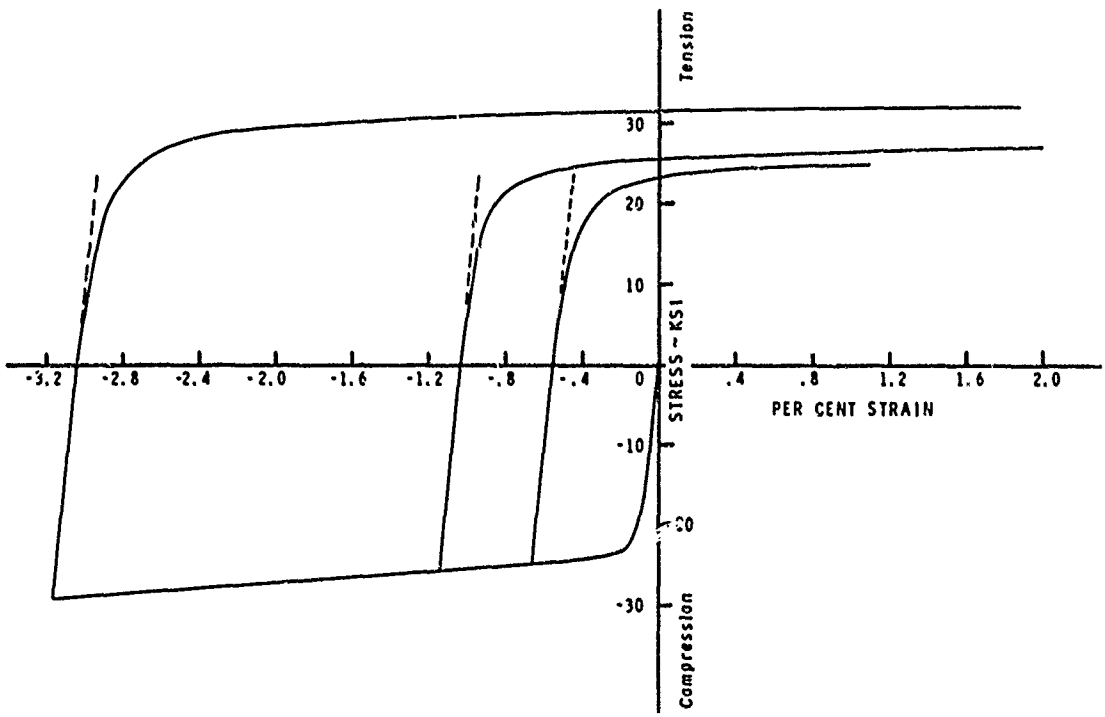

Figure 5 Reverse Loading Behavior, Tantalum

Cyclic loading behavior is shown in Figure 6 where a single specimen was put in compression and then tension through a total of 5 cycles. The observed yield and flow stress behavior is indicative of an isotropic hardening mechanism.

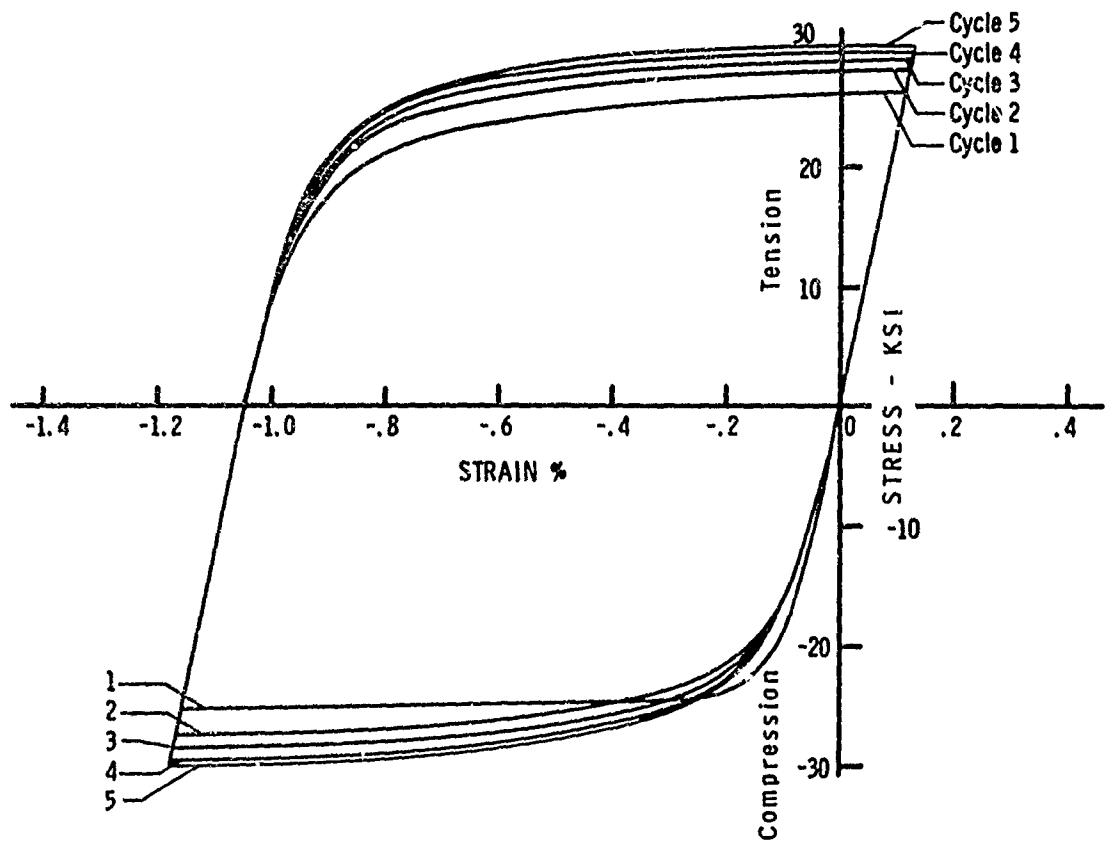

Figure 6 Cyclic Loading Behavior, Tantalum

SECTION III

ELASTIC BEHAVIOR

Measurement of elastic constants provides additional inputs to the study of material response. Three basic measurements are density, longitudinal (dilatational) wave velocity and shear (transverse) wave velocity. Measurements of temperature and pressure dependence of the wave velocities lead to prediction of pressure-compression isotherms, adiabats and hydrostats. If these measurements are made with sufficient accuracy ($\sim$0.1%), the calculated pressure-compression behavior can frequently be extrapolated with reasonable confidence to higher pressures than covered in the actual measurements.

WAVE VELOCITY MEASUREMENTS

Initial measurements of longitudinal and shear wave velocities were made at 20°C and atmospheric pressure (i.e., P = 0). Values obtained parallel to the bar axis were:

$$C_L = 4.146 \pm 0.005 \text{ mm/}\mu\text{sec}$$

$$C_S = 2.032 \pm 0.003 \text{ mm/}\mu\text{sec}$$

Although the accuracy of these measurements are estimated to be about $\pm$ 0.1%, it should be noted that C_L and C_S may vary depending on the structural form of the material (i.e., plate, bar, etc.), its thermal and mechanical history, and the measurement direction relative to any structural anisotropy.

Measurements were made of temperature and hydrostatic pressure dependence of wave velocities and the data corrected for thermal expansion and hydrostatic compression to give:

Temperature Dependence, 0-100°C, P = 0

$C_L = 4.149 - 0.000146T$ mm/μsec

$C_S = 2.036 - 0.000173T$ mm/μsec

(T in °C)

Pressure Dependence, 0-9 kbar, T = 20°C

$C_L = 4.146 + 0.00291P$ mm/μsec

$C_S = 2.032 + 0.00137P$ mm/μsec

(P in kbar)

Temperature and pressure dependence of elastic constants for single-crystal tantalum have been reported by Soga[20] and Chechile,[21] and Palmieri[22] and Armstrong and Brown[23] have published data on temperature dependence of elastic constants in polycrystalline tantalum. Palmieri also found C_E (sound wave velocity) to vary from 3.245 to 3.366 mm/μsec and C_S from 2.035 to 2.085 mm/μsec (at 0°C), depending on specimen orientation and heat treatment (i.e., annealing). Lamberson[24] studied both temperature and pressure dependence of C_L and C_S in polycrystalline tantalum with a density of 16.64 g/cc and 16 to 30 μm grain size. C_L was given as $4.156-0.0001573T$ and $4.153 + 2.0025P$, and C_S as $2.037 - 0.0001418T$ and $2.034 + 0.0010P$ (T in °C and P in kbar).

ELASTIC CONSTANTS

Assuming polycrystalline tantalum* is isotropic (C_L and C_S are independent of direction of measurement in a polycrystalline specimen), wave velocity data can be used to calculate various elastic constants. At 20°C and zero pressure, the following adiabatic constants were obtained:

Bulk wave velocity, C_B = 3.42 mm/μsec
Sound wave velocity, C_E = 3.33 mm/μsec
Rayleigh wave velocity, C_R = 1.90 mm/μsec
Poisson's ratio, ν = 0.342
Bulk modulus, K = 1946 kbar
Shear modulus, G = 688 kbar
Elastic modulus, E = 1846 kbar
Lamé's parameter, λ = 1488 kbar

The adiabatic bulk and shear moduli were obtained as functions of T and P from the following:

$$K = \rho \left(C_L^2 - \frac{4}{3} C_S^2 \right)$$

$$G = \rho C_S^2$$

* A cubic material is elastically isotropic when $\frac{2C44}{C_{11}-C_{12}} = 1$, where C_{44}, C_{11} and C_{12} are elastic stiffness constants. Single-crystal tantalum is slightly anisotropic with $\frac{2C44}{C_{11}-C_{12}} \approx 1.56$ [20,25,26].

This gave:

Temperature dependence, P = 0

$K^S = 1948 - 0.084T$ kbar

$G^S = 691 - 0.131T$ kbar

Pressure dependence, T = 20°C

$K^S = 1946 + 3.79P$ kbar

$G^S = 688 + 1.28P$ kbar

where the superscript S indicates adiabatic.

Isothermal values of K and G as well as adiabatic and isothermal pressure and temperature derivatives at 20°C and zero pressure were calculated and results are given in Table I. Use of these constants in calculating the isotherm, adiabat and hydrostat is discussed in the section on Equation of State.

GRUNEISEN PARAMETER

The Gruneisen ratio γ is a parameter in the solid equation of state relating pressure to volume and energy, $\gamma = V\,(\partial P/\partial E)_V$ (see, e.g., Ref. 27). This parameter can be expressed thermodynamically as:

$$\gamma = -\frac{1}{\rho c_p}\left(\frac{\partial V}{\partial T}\right)_P\left(\frac{\partial P}{\partial V}\right)_S = \frac{\beta k^S}{\rho c_p} \qquad (1)$$

TABLE I

ELASTIC CONSTANTS FOR TANTALUM
(P = 0, T = 20°C)

PARAMETER	VALUE
K^S	1946 kbar
$(\frac{\partial K^S}{\partial P})_T = K_{0T}^{S'}$	3.79
$(\frac{\partial K^S}{\partial T})_P$	- 0.084 kbar/°C
$(\frac{\partial K^S}{\partial P})_S = K_{0S}^{S'}$	3.77
$(\frac{\partial K^S}{\partial T})_S$	15.1 kbar/°C
K^T	1928 kbar
$(\frac{\partial K^T}{\partial P})_T = K_{0T}^{T'}$	3.80
$(\frac{\partial K^T}{\partial T})_P$	- 0.146 kbar/°C
$(\frac{\partial K^T}{\partial P})_S = K_{0S}^{T'}$	3.77
$(\frac{\partial K^T}{\partial T})_S$	15.1 kbar/°C
$G^S = G^T$	686 kbar
$(\frac{\partial G}{\partial P})_T = G_{0T}'$	1.28
$(\frac{\partial G}{\partial T})_P$	- 0.131 kbar/°C
$(\frac{\partial G}{\partial P})_S = G_{0S}'$	1.25
$(\frac{\partial G}{\partial T})_S$	5.02 kbar/°C

For an isotropic elastic solid, this gives:

$$\gamma = \frac{\beta}{c_p} \left(c_L^2 - \frac{4}{3} c_S^2 \right) \tag{2}$$

where C_L and C_S are measured under adiabatic conditions.

At 20°C and zero pressure:

$$\gamma_0 = 1.63$$

The zero-pressure Gruneisen parameter can also be estimated by several other methods, including those of Slater[28], Dugdale and MacDonald[29], Anderson and Dienes[30,31], and Schuele and Smith[30,32]. These methods are discussed in Appendix A.

An estimate of the temperature dependence of the Gruneisen parameter can be obtained by differentiating Equation 1 with respect to temperature. At constant pressure (P = 0, T = 20°C):

$$\left(\frac{\partial \gamma}{\partial T}\right)_P = \gamma_0 \left[\frac{1}{\beta} \left(\frac{\partial \beta}{\partial T}\right)_P + \frac{1}{K^S} \left(\frac{\partial K^S}{\partial T}\right)_P - \frac{1}{\rho} \left(\frac{\partial \rho}{\partial T}\right)_P - \frac{1}{c_p} \left(\frac{\partial c_p}{\partial T}\right)_P \right] = -0.00043/°C \tag{3}$$

The pressure dependence can be estimated by differentiating with respect to pressure. At constant temperature (T = 20°C, P = 0):

$$\left(\frac{\partial\gamma}{\partial P}\right)_T = \frac{\gamma_0}{K^S}\left[\left(\frac{\partial K^S}{\partial P}\right)_T + \frac{1}{\beta K^T}\left(\frac{\partial K^S}{\partial T}\right)_P - 1 - \gamma - T\left(\frac{\partial\gamma}{\partial T}\right)_P\right] = -0.00077/\text{kbar} \qquad (4)$$

Another approach is to assume γ/V constant, which permits $(\partial\gamma/\partial P)_T$ to be estimated directly from the bulk modulus data. At constant temperature (20°C):

$$\left(\frac{\partial\gamma}{\partial P}\right)_T = \frac{-\gamma_0}{\left(\frac{1}{K_0^T}\right)^{\left(1/K_{0T}^{T'}\right)}\left(K_0^T + K_{0T}^{T'}P\right)^{\left(1+K_{0T}^{T'}\right)/K_{0T}^{T'}}}$$

$$= \frac{-11.93}{(1928+3.8P)^{1.263}} \qquad (5)$$

$$= -0.00085/\text{kbar} \text{ @ } P = 0$$

DEBYE TEMPERATURE

The Debye temperature θ is important in thermal energy calculations and indicates the temperature above which variations due to temperature for some thermodynamic parameters such as specific heat, thermal expansion and Gruneisen ratio become small. There are a number of methods for calculating the Debye temperature[33], and one approximation suitable for use

with elastic wave velocity data for polycrystalline metals is:

$$\theta = \frac{h}{k} \left(\frac{9N}{4\pi V}\right)^{1/3} \left(\frac{1}{C_L^3} + \frac{2}{C_S^3}\right)^{-1/3}$$

where h is Planck's constant, k is Boltzmann's constant, N is number of mass points and V is sample volume.

At 20°C, the elastically-determined Debye temperature for tantalum is:

$$\theta = 4.3 \times 10^{-5} \left(\frac{N}{V}\right)^{1/3} \left(\frac{1}{C_L^3} + \frac{2}{C_S^3}\right)^{-1/3} \qquad (6)$$

$\theta = 260°K$

for N = 2 (atoms per unit cell), $V = (3.306 \times 10^{-7}\text{mm})^3$ (lattice constant)[34], C_L = 4.146 mm/μsec and C_S = 2.032 mm/μsec.

SECTION IV

EQUATION OF STATE

The development of material response models and computational codes requires data on material behavior under uniaxial strain conditions, including equation of state, wave propagation and spall fracture. Most data are used directly in developing models of material behavior, although independent check data (attenuated wave and spall wave profiles) are necessary to determine accuracy of the calculations. This section presents equation of state analyses, and the following two sections cover wave propagation and spall fracture.

SHOCK WAVE EQUATION OF STATE

The hugoniot equation of state is the locus of equilibrium states reached after shocking of a material, and data are usually obtained either as stress-particle velocity points or as shock velocity-particle velocity points. The hugoniot data presented in this report were obtained with x-cut quartz gages and representative records for direct impact and transmitted wave tests are shown in Figure 7. The buffered direct impact method (tungsten carbide buffer plate on front of the quartz) permitted stresses up to 80 kbar in tantalum while keeping the stress in quartz at an acceptable level. The use of quartz gages for transmitted wave tests was primarily for the study of compressive wave development and elastic precursor decay, and results are discussed in the Wave Propagation section.

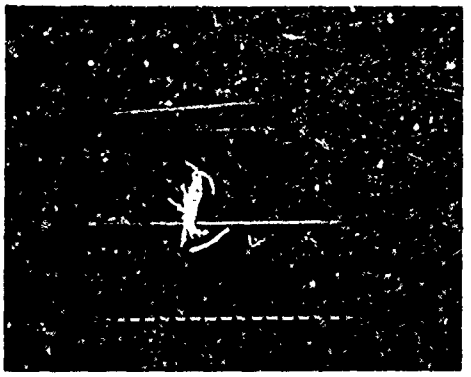

DIRECT IMPACT

Ta → Q

V_I = 0.164 mm/μs

σ_H = 20.8 kbar

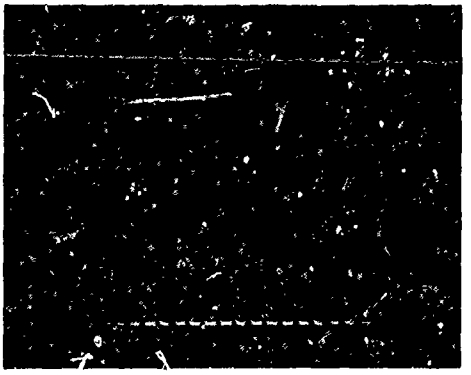

DIRECT IMPACT, BUFFERED

Ta → WC/Q

V_I = 0.159 mm/μs

σ_H = 60.8 kbar

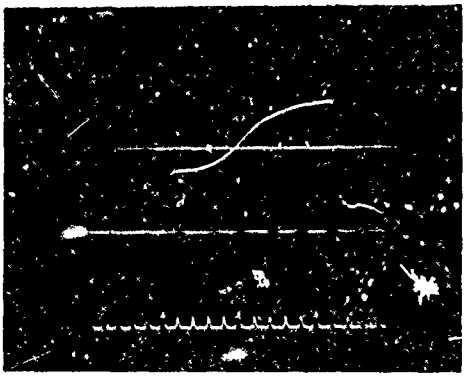

TRANSMITTED WAVE

Al → Ta/Q

V_I = 0.269 mm/μs

σ_s = 32.8 kbar

Figure 7 Quartz Gage Records

The direct impact records showed very fast rise times (<10 nsec) and then a straight peak stress region. The slight rounding at the front of the direct impact records in Figure 7 is due to impact tilt, and the ramped peak stress region results from finite-strain effects in the quartz which are corrected in the data analysis.[35]

The hugoniot may be expressed in several forms. A convenient form for experimental work is that established by a least-squares fit to data in the stress-particle velocity ($\sigma_H - u_p$) plane. Transformation of the hugoniot into other planes, such as shock velocity-particle velocity ($U_S - u_p$) or stress-volume ($\sigma_H - v$), is performed by assuming a material model. This was done by assuming an ideal elastic-plastic wave structure with equilibrium initial and final states and applying the mass and momentum conservation equations:

$$\sigma_H = \sigma_e + \rho_e (U_S - u_e) (u_p - u_e) \tag{7}$$

and

$$v = v_o \left(1 - \frac{u_e}{C_L}\right) \left(\frac{U_S - u_p}{U_S - u_e}\right) \tag{8}$$

where ρ_e and u_e are density and particle velocity at the elastic limit σ_e.

Therefore, when either $\sigma_H - u_p$ or $U_S - u_p$ relations are established and σ_e, ρ_e, u_e and C_L are known, σ_H, U_S, u_p and v are uniquely determined. The resulting hugoniots for tantalum at 20°C are given in Figures 8, 9, and 10, and are listed below:

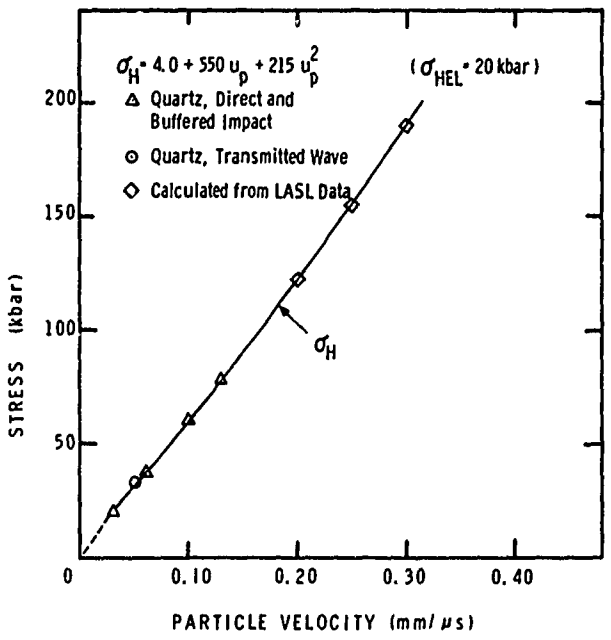

Figure 8 Stress-Particle Velocity Hugoniot, Tantalum

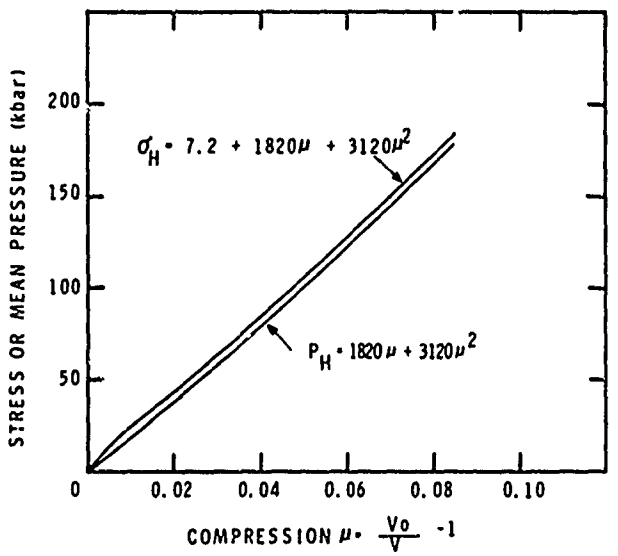

Figure 9 Stress or Mean Pressure-Compression Hugoniot, Tantalum

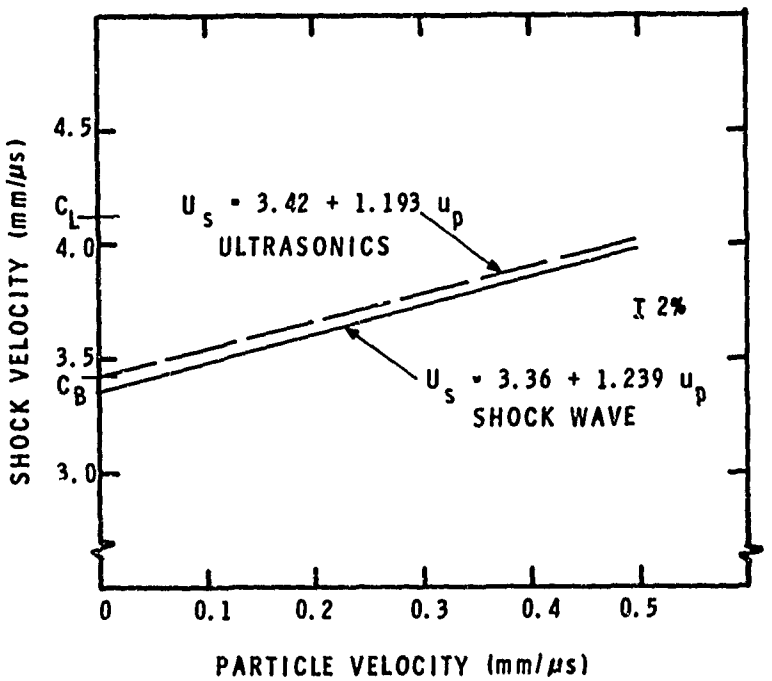

Figure 10 Shock Velocity-Particle Velocity Hugoniot, Tantalum

$$\left.\begin{aligned} \sigma_H &= 4.0 + 550\ u_p + 215\ u_p^2 \quad \text{(Std. Error 0.3 kbar)} \\ \sigma_H &= 7.2 + 1820\ \mu + 3120\ \mu^2 \\ P_H &= 1820\ \mu + 3120\ \mu^2 \quad \text{(Hydrostat)} \\ U_S &= 3.36 + 1.239\ u_p \end{aligned}\right\} \quad (9)$$

where $\mu = (v_o/v - 1)$

These equations are based on the data points indicated by the symbols in Figure 8 and on σ_e = 20 kbar, and are considered to be valid over the stress range of 20 to 200 kbar.* Accuracy of the quartz gage data is estimated as ± 2% for

σ_H and ± 1% for u_p. Hugoniot points reported by Rohde and Towne[37] for 99.9% polycrystalline tantalum at 30.2, 43.1, 48.8 and 85.8 kbar are within + 1%, - 8% of the fit to the data given in Figure 8.

The hydrostat (P_H-μ) was obtained by subtracting the stress-axis intercept value from the σ_H-μ equation. This approach satisfies the requirement that the P_H-μ function pass through the origin and assumes the deviatoric stress (σ_D) is constant (no strain hardening). Alternative ways of estimating σ_D for the low-pressure region are discussed in Appendix B.

ULTRASONIC EQUATION OF STATE

The equation of state can also be determined from ultrasonics measurements. Accurate measurement of elastic wave velocities (and, therefore, bulk modulus) as a function of hydrostatic pressure makes it possible to directly estimate shock wave compression behavior. Numerous analytical and empirical relations have been developed for relating pressure, volume and bulk modulus, including those of Birch[38,39], Murnaghan[40] and Keane[41,42]. The use of these relations is discussed in Appendix C and results are summarized below:

Birch EOS

$$P_T = 2891 \left[(1+\mu)^{7/3} - (1+\mu)^{5/3}\right]\left[1-0.15\left\{(1+\mu)^{2/3}-1\right\}\right] \quad (10)$$

* The hugoniot was extended to 200 kbars by including three calculated points obtained from the high-pressure U_S-u_p hugoniot given in Reference 36. This hugoniot was converted to the σ_H-u_p plane after assuming a hugoniot elastic limit of 20 kbar, and three σ_H-u_p "points" were then calculated at particle velocities of 0.20, 0.25 and 0.30 mm/μsec.

Murnaghan EOS, Isotherm

$$P_T = 507.1 \left[(1+\mu)^{3.80} - 1 \right] \tag{11}$$

Murnaghan EOS, Adiabat

$$P_S = 516.2 \left[(1+\mu)^{3.77} - 1 \right] \tag{12}$$

Keane EOS, $K_\infty^{S'} = 3.6$

$$P_S = 566.1 \left[(1+\mu)^{3.6} - 1 \right] - 91.9 \ln (1+\mu) \tag{13}$$

Keane EOS, $K_\infty^{S'} = 1.10$

$$P_S = 6063 \left[(1+\mu)^{1.10} - 1 \right] - 4723 \ln (1+\mu) \tag{14}$$

In the above equations, subscripts T and S indicate isothermal and isentropic, respectively.

Duvall gives a method of calculating the increase in entropy across a shock which can be applied to the Murnaghan equation to give:[24,43]

$$P_H = P_S + \frac{\gamma_0 K_0^S}{12} \left(K_{0S}^{S'} + 1 \right) \left(\frac{\mu}{1+\mu} \right)^3$$

$$P_H = P_S + 1261 \left(\frac{\mu}{1+\mu} \right)^3 \tag{15}$$

Zel'dovich gives an expression relating P_S and P_T, assuming γ/v is constant:[24,44]

$$P_S = P_T + \beta T_0 K_0^T \left[\exp \left\{ \gamma_0 \left(\frac{\mu}{1+\mu} \right) \right\} - \left(1+\mu \right) \right] \qquad (16)$$

$$P_S = P_T + 10.4 \left[\exp \left\{ 1.63 \left(\frac{\mu}{1+\mu} \right) \right\} - \left(1+\mu \right) \right]$$

The above equations of state are compared to the shock wave EOS in Table II. The entropy correction based on the Murnaghan equation has been applied to the Birch and Keane equations as well. The ultrasonic equations of state show good agreement with each other but are 3 to 6% above the shock wave hydrostat.

The shock velocity-particle velocity relationship can also be determined from ultrasonic data. Following the method of Ruoff[45] one obtains:

$$U_S = C_B + S u_p + A u_p^2 \qquad (17)$$

$$\left.\begin{aligned} \text{where } C_B &= \left(\frac{K_0^S}{10 \rho_0} \right)^{1/2} \\ S &= 1/4 \left(K_{0S}^{S'} + 1 \right) \\ A &= \frac{1}{24\, C_B} \left[S \left(7 - K_{0S}^{S'} + 4\gamma_0 \right) + 2 K_0^S K_{0S}^{S''} \right] \end{aligned}\right\} \qquad (18)$$

TABLE II

EQUATIONS OF STATE COMPARISON-HYDROSTAT, TANTALUM

$\mu = \frac{V_o}{V} - 1$	P_H, HUGONIOT MEAN PRESSURE (kbar)					
	BIRCH	MURNAGHAN		KEANE		SHOCK WAVE
	EQ. 10	EQ. 11	EQ. 12	EQ. 13	EQ. 14	EQ. 9
0.02	39.7	39.7	40.0	40.0	40.0	37.6
0.04	81.8	81.9	82.4	82.3	82.2	77.8
0.06	126.0	126.3	127.0	127.0	126.3	120.4
0.08	172.7	173.3	174.3	174.2	172.6	165.6
0.10	221.6	222.8	224.1	223.9	220.9	213.2

For tantalum:

$$U_S = 3.42 + 1.193\ u_p + 0.14\ u_p^2$$

The u_p^2 coefficient (A = 0.14) was calculated assuming $K_{OS}^{S"} = 0$. If one assumed A = 0, then $K_{OS}^{S"} = -0.003$. Since the uncertainty in $K_{OS}^{S"}$ is on the order of $\pm$ 0.01, the A coefficient will be taken as zero, which gives:

$$U_S = 3.42 + 1.193\ u_p \qquad (19)$$

This is compared with the linear $U_S - u_p$ relation obtained from low-pressure shock wave data in Figure 10.

Vaidya and Kennedy measured the hydrostatic compressibility of 99.99% polycrystalline tantalum rod up to 45 kbar.[46] Results were given as

$$-\frac{\Delta v}{v_o} = \frac{\mu}{1+\mu} = 0.4953 \times 10^{-3} P_T - 0.59394 \times 10^{-6} P_T^2 \qquad (20)$$

Comparing this with the shock wave and ultrasonics results presented in this report gives:

P_T, ISOTHERMAL PRESSURE (kbar)

μ	Shock Wave Eq. 9*	Ultrasonics Eq. 11	Hydrostatic Eq. 20
0.005	9.2	9.7	10.2
0.010	18.5	19.5	20.5
0.015	27.9	29.5	31.0
0.020	37.5	39.6	41.6

* Corrected for isothermal conditions.

The hydrostatic data of Vaidya and Kennedy are 5 to 10% above ($P_T - \mu$ plane) the shock wave and ultrasonic data.

YIELD BEHAVIOR

A complete description of the low-pressure equation of state requires consideration of yield behavior or the hugoniot elastic limit. Values of compressive yield were obtained by three independent methods.

A. Uniaxial Stress

The yield level was determined in uniaxial stress (σ_σ) as a function of strain rate and then converted to unaxial strain using:

$$\sigma_e = \sigma_\sigma \left(\frac{1-\nu}{1-2\nu}\right) \tag{21}$$

Strain Rate (sec^{-1})	σ_e (kbar)
800	11.2
10^{-3}	2.9

B. Wave Profiles

The elastic precursor level was measured as a function of propagation distance using quartz gages. These profiles are discussed in the section on Wave Propagation.

Propagation Distance (mm)	σ_e (kbar)
2	19
12	16

C. Hugoniots

The yield level in uniaxial strain was inferred by comparison of the elastic ($\rho_0 C_L$) and plastic (σ_H vs. u_p) hugoniots, i.e., by defining the elastic limit as the intersection of the elastic response line and the curve-fit to the stress-particle velocity data

$$10\ \rho_0 C_L u_e = A + Bu_e + Cu_e^2$$

Solving for u_e gives

$$u_e = 0.029 \text{ mm/}\mu\text{sec}$$

$$\therefore\ \sigma_e = 20.0 \text{ kbar}$$

For an isotropic, polycrystalline metal with elastic-perfectly plastic behavior and no strain-rate or time-dependent effects, one would expect the same yield to be obtained by each method. The yield obtained from wave profile tests and the hugoniot measurements are in fair agreement, but are both much higher than the yield determined from uniaxial stress data for rates less than 10^3/sec. For this particular tantalum, the equilibrium yield in uniaxial strain was assumed to be 20 kbar for use in the EOS transformations made in obtaining the $\sigma_H - \mu$ and $U_S - u_p$ relations given above (Equation 9).

SECTION V

WAVE PROPAGATION

Profiles of shock waves propagated through a specimen were recorded as stress-time or velocity-time histories. The stress-time data were obtained with quartz gages and the results were transformed to material stress by application of an impedance matching technique,[35] assuming time-independent behavior. The velocity-time data were obtained with a velocity interferometer and are presented as measured. All wave profiles obtained are given in Appendix D for reference.

COMPRESSIVE WAVE BEHAVIOR

Structure in the compressive wave is shown in the quartz gage data in Figure 11.* The wave front is characterized by an elastic portion and a transition to a spreading plastic wave (nominal final stress of 34 kbar). (The elastic wave would be overdriven by the plastic wave at ∿ 440 kbar).

Also shown in Figure 11 are shock velocities as calculated from the shock wave hugoniot (Equation 9). Although the calculated plastic wave velocity lies within the rise-time of the measured wave, the plastic wave is not a step pulse and shows spreading with propagation distance at this stress

* In this and subsequent figures containing quartz gage data, tilt refers to the time required for a step-input to sweep across the gage electrode diameter.

level. This means that transformation of the hugoniot from the $\sigma_H - u_p$ plane to $\sigma_H - u$ or $U_S - u_p$ by assuming ideal elastic-plastic wave structure and steady-state conditions may lead to some uncertainty at lower stresses.

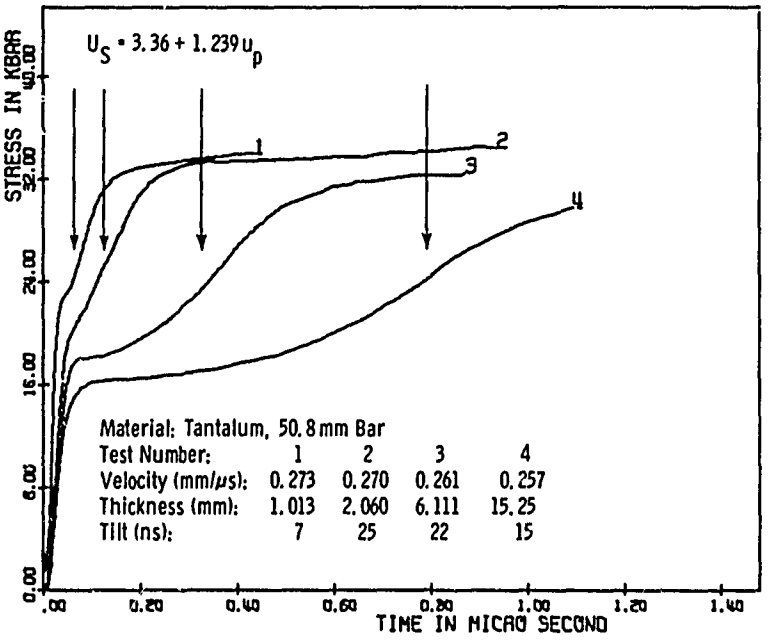

Figure 11 Compressive Waves, Propagation Distance Dependence (6061-T6 Al Impactors)

Two tests with quartz gages were conducted using specimens machined from a piece of 76.2 mm diameter bar, and results are compared to 50.8 mm bar data in Figures 12 and 13. Although the 76.2 mm bar was ordered to the same nominal specifications as the 50.8 mm bar*, the compressive wave development is significantly different. The larger diameter bar showed a less well-defined elastic limit but a "faster" plastic wave. These differences can probably be attributed to changes in metallurgical characteristics of the material.

* Impurity content for the 76.2 mm bar was about the same as the 50.8 mm, but the yield and flow stress at low strain rate was about twice as high and hardness was 86 R_K.

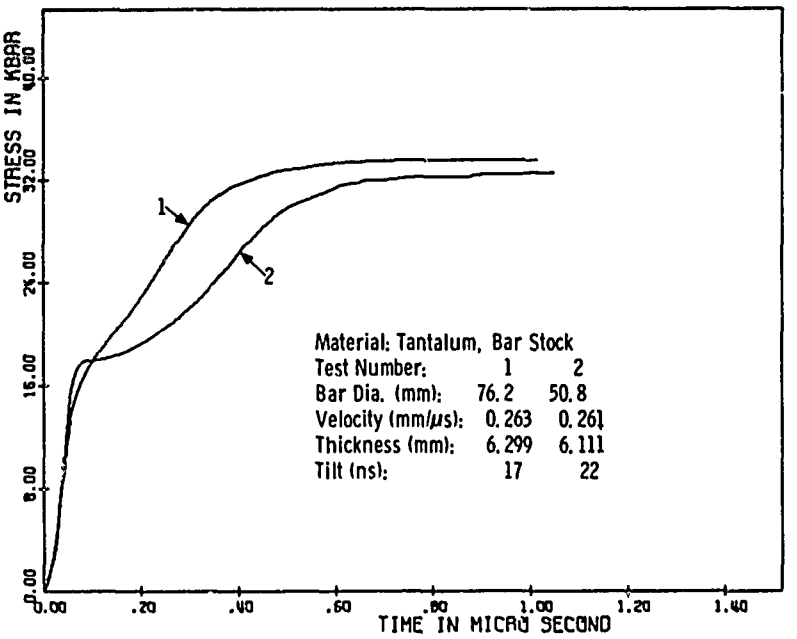

Figure 12 Compressive Waves, Material Differences (6061-T6 Al Impactors)

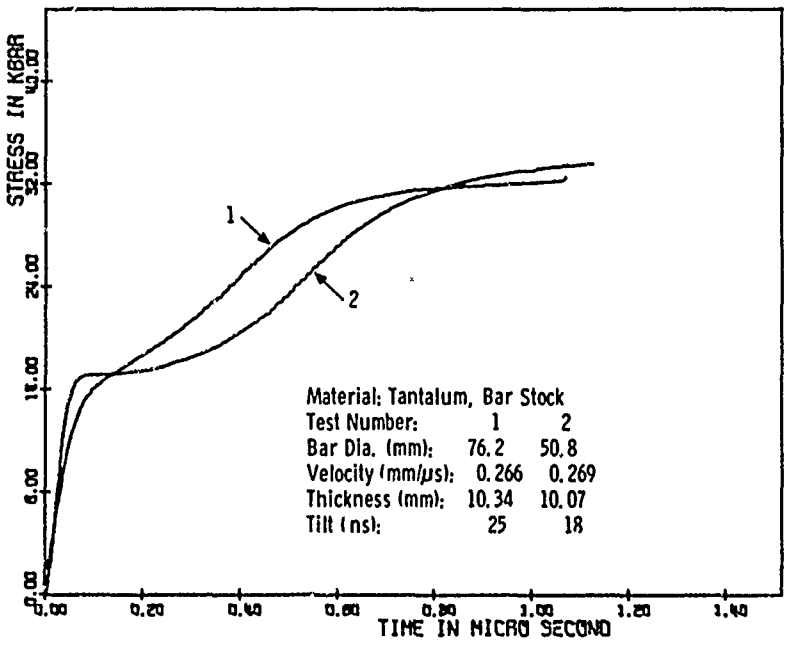

Figure 13 Compressive Waves, Material Differences (6061-T6 Al Impactors)

Precursor decay data for tantalum, as determined from quartz gage data, is summarized in Figure 14. The calculated initial elastic impact stress was ∿ 37 kbar for these tests and the precursor level has dropped ∿ 50% in 2 mm of travel. The equilibrium or steady-state elastic limit appears to be ∿ 15 kbar. The uncertainty bars in Figure 14 reflect dispersion and rounding at the elastic front which is due to at least three factors. First, since quartz gages average stress over the electrode area, small differences in wave front arrival times at the specimen/gage interface would give a finite rise-time rather than an instantaneous stress jump. Second, the finite thickness of the epoxy between the specimen and the gage will increase the apparent rise-time in the wave front. Third, the influence of shock wave tilt on a finite-area gage is to smooth out abrupt changes in stress level as well as to increase recording rise-time of the wave front.

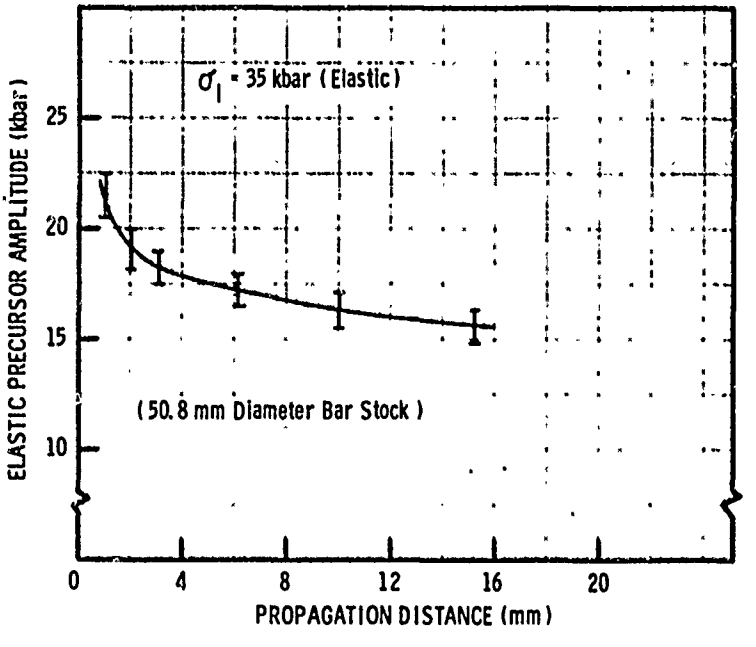

Figure 14 Elastic Precursor Decay in Tantalum

Gillis, et al.,[47] reported elastic precursor decay data for annealed, high-purity (99.9%) tantalum. Direct comparison with the present work is not possible because of material differences and variations in impact stress and propagation distance, however, their data tend toward the same steady-state yield value, 15 kbar. Gillis, et al., used quartz gages to record the stress profiles and indicated elastic wave rise-times on the order of 100 nsec, after correction for tilt. The quartz gage data shown in Figure 11 (not corrected for tilt), show rise-times generally less than 50 nsec, and velocity interferometer data, discussed below, showed rise-times to be less than 20 nsec.

To determine if rise-time of the input pulse influenced precursor development, a series of velocity interferometer tests were performed with a fused quartz buffer on the front of the tantalum target. (Test conditions for all velocity interferometer tests discussed in this report are listed in Table III). Because of the nature of the fused quartz hugoniot at stresses below ∿ 40 kbar,[48] the compressive wave spreads as it propagates. The rise-time of the pulse at the fused quartz/tantalum interface was ∿ 300 nsec and the resulting compressive wave profiles after propagation through several thicknesses of tantalum are shown in Figure 15. The calculated elastic limits at 6 and 10 mm (18 and 16 kbar, respectively) are approximately the same as those determined from the quartz gage tests. This indicates that elastic wave development is insensitive to input pulse rise-time (i.e., strain rate), at least for rise-times of 300 nsec or less. Note that Test 225 in Figure 15 shows evidence of a slight yield drop or stress relaxation. Although this behavior might be expected on the basis of the relaxation observed in the uniaxial stress tests (see Figure 3), it was seen on only two velocity interferometer tests and on none of the quartz gage tests.

TABLE III

VELOCITY INTERFEROMETER TEST DATA, TANTALUM

Test No.	V_I Impact Velocity (mm/μs)	Max. Stress (kbar)	X_0 Impactor Thickness (mm)	X Target Thickness (mm)	X/X_0	Config.[1]
154	0.269	82	1.488	4.552	3.06	Ta-Ta
155	0.218	66	1.483	4.417	2.98	Ta-Ta
156	0.125	39	1.473	4.562	3.10	Ta-Ta
168[2]	0.228	69	0.599	1.519	2.54	Ta-Ta/FQ
169[2]	0.216	66	0.594	3.022	5.09	Ta-Ta/FQ
170[2]	0.225	69	0.617	5.057	8.20	Ta-Ta/FQ
171[2]	0.215	66	0.615	10.11	16.44	Ta-Ta/FQ
172	0.205	63	0.632	1.534	2.43	Ta-Ta/FQ
180	0.332	101	0.645	4.534	7.03	Ta-Ta
224	0.293	33	12.7	12.72/1.946	--	Al-FQ/Ta/FQ
225	0.283	33	12.7	12.71/6.121	--	Al-FQ/Ta/FQ
226	0.286	33	12.7	12.72/10.15	--	Al-FQ/Ta/FQ

1. E.g., Ta-Ta is tantalum impactor into tantalum target with free rear surface (FQ is fused quartz window).
2. Lexan-backed impactor.

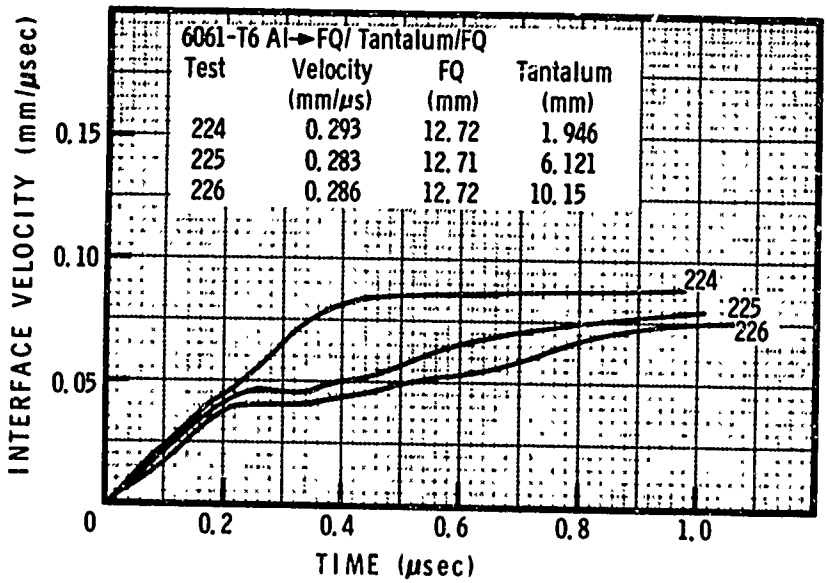

Figure 15 . Compressive Waves, Long Rise-Time Input Pulse

RELEASE WAVES AND WAVE ATTENUATION

Release waves were studied by using relatively thin impactors and measuring the complete wave profile with the laser velocity interferometer. Unattenuated wave profiles are shown in Figure 16 for unbacked (free rear surface) and Lexan-backed impactors.* The unloading wave in tantalum is dispersive but does not show a distinct elastic-plastic structure. Although the final interface velocity is higher for the Lexan-backed impactor due to the incomplete unloading, the slope of the rarefaction waves are essentially the same. This result is significant since the attenuation results discussed below are for Lexan-backed impactors.

* Lexan is a polycarbonate sheet made by General Electric Co. and has a density of 1.20 g/cc. An approximate equation of state determined for use in wave propagation calculations is $\sigma_H \simeq 31\ u_p + 15\ u_p^2$.

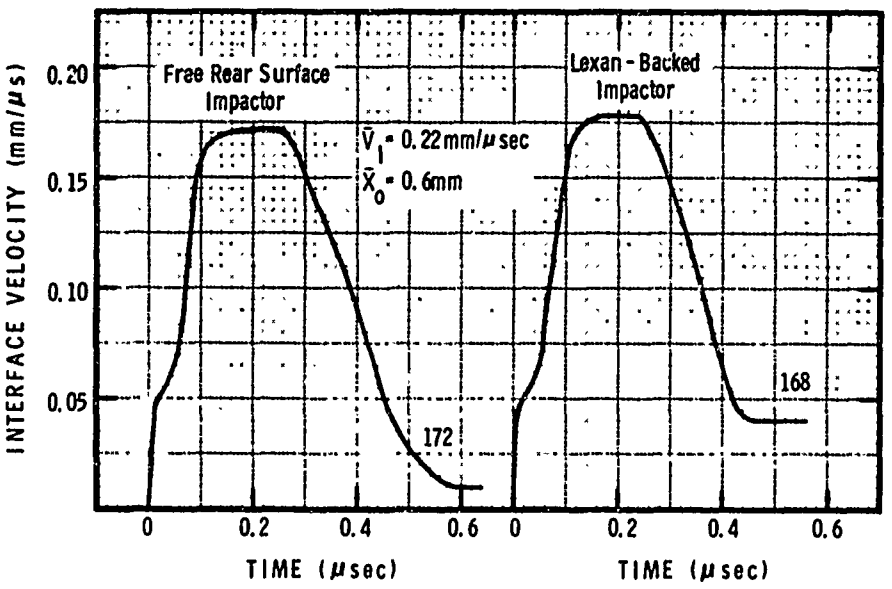

Figure 16 Complete Wave Profiles, Tantalum

If target thickness is large enough compared to impactor thickness, the release wave will overtake the compressive wave and attenuate the peak stress, as shown in Figure 17. The initial stress was ∿ 69 kbar and the impactors were backed with Lexan which gave only ∿ 80% unloading. The overtaking point can be calculated assuming ideal elastic-plastic compression and release waves, which gives:

$$\frac{X}{X_0} \simeq \frac{\frac{1}{C_L} + \frac{1-u_p/U_S}{C_L^1-u_p}}{\frac{1}{U_S} - \frac{1-u_p/U_S}{C_L^1+u_p}} \qquad (22)$$

where C_L^1 is elastic release wave velocity (assumed to be 4.3 mm/μs for 69 kbar).

At 69 kbar, $u_p \sim 0.11$ mm/μs and $U_S \sim 3.5$ mm/μs from Equation 9. This gives $X/X_o = 7.9$ which is larger than actually measured. This can be attributed to the ramped plastic compressive wave at this stress. If the velocity (∿ 3.1 mm/μs) of the trailing portion of the plastic wave is used for U_S rather than the value obtained from Equation 9, the calculated overtaking point is $X/X_o = 4.8$. This is in better agreement with the experimental results shown in Figure 17.

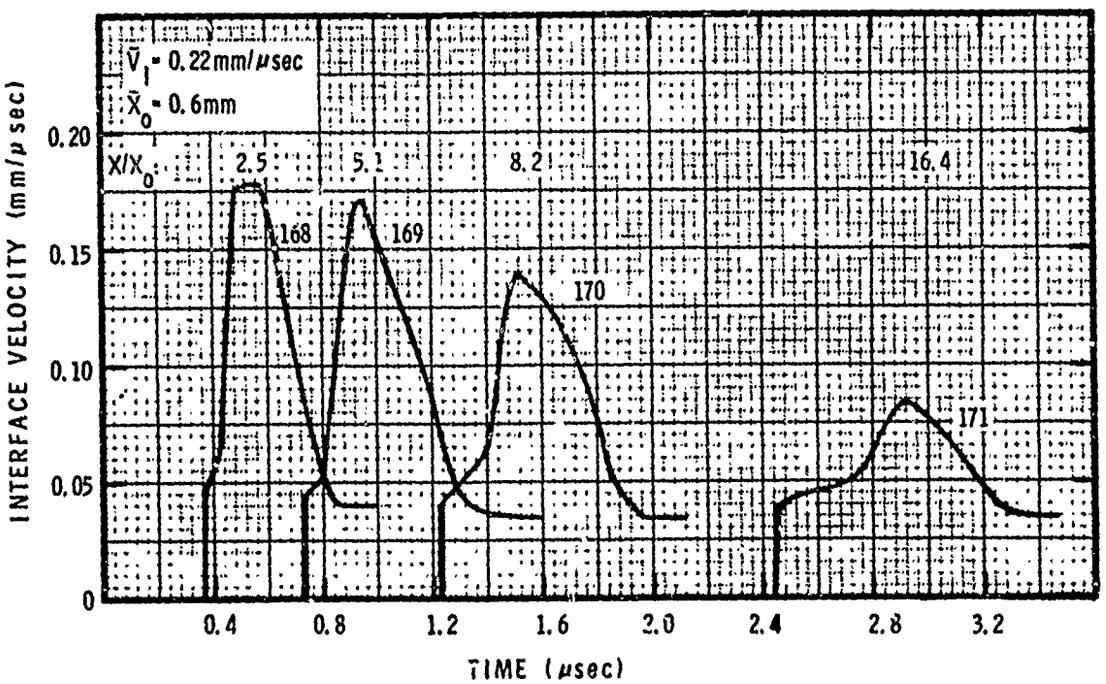

Figure 17 Wave Attenuation in Tantalum

SECTION VI

SPALL FRACTURE

Spall fracture by plate impact results from reflection of compressive waves from a relatively low impedance interface (normally a free surface) and subsequent wave interaction. Spall studies were carried out with both passive and active techniques. Passive methods involve the recovery and examination of shock-loaded specimens. Metallographic examination establishes the type and degree of damage, which can be correlated with test parameters such as velocity, impactor thickness and target thickness. Active methods utilize the laser velocity interferometer and provide time-resolved data on the influence of spall fractures on shock wave profiles, as measured at the rear surface.

RECOVERY TESTS

Spall behavior of tantalum was studied by carrying out a series of impact and recovery tests,* where the target was sectioned across a diameter, polished, etched, and examined optically at a magnification of 50X. The specimens were then graded or classified according to the degree of fracture that was observed, which ranged from no visible damage to complete material separation. The onset of significant fracture is generally referred

* Hanneman[49] studied the thermal spall behavior of tantalum using a capacitor discharge technique. He reported a "spall threshold temperature" of 1900 to 2140°C for tantalum wire.

to as incipient spall and is a critical point since it can be used to deduce dynamic fracture strength, and corresponds to generation of sufficient free surface area within the material to reflect a portion of the interacting release waves as a compressive wave. The incipient spall threshold was defined as the impact velocity (for a given set of impact parameters) corresponding to cracking over at least 50% of the width of the section estimated to be under a condition of plane strain during the time of loading.

Incipient spall velocity results are summarized in Table IV and the data are given in Figure 18. The symbols are defined as:

- ● Complete Separation
- ⊖ Above Incipient
- ⊗ Incipient Spall
- ⊖ Below Incipient
- O No Visible Damage

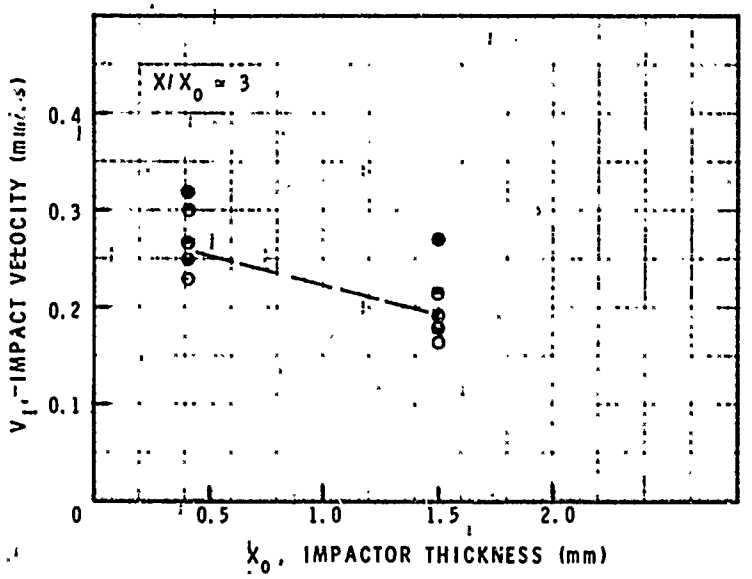

Figure 18 Spall Data for Tantalum

TABLE IV

INCIPIENT SPALL DATA, TANTALUM (20°C)

X_0 Impactor Thickness (mm)	X Target Thickness (mm)	X/X_0	Δt_e Pulse Width* (μs)	V_S Spall Velocity (mm/μs)
0.41	1.27	3.10	0.198	0.260
1.50	4.54	3.03	0.724	0.190
0.57	4.60	8.07	0.275	0.320

* $\Delta t_e = \frac{2X_0}{C_L}$

As is typically the case with metals, the impact velocity for incipient spall increases for decreasing impactor thickness. This implies that peak stress (and therefore strain) required to create spall fractures increases with decreasing pulse width or time of loading. Optical photomicrographs of recovered specimens are shown in Figures 19 and 20.* The specimens were polished and etched to provide maximum contrast between cracks and sound material. The procedure followed was:

1. Wet grind, 320/400/600 grit silicon carbide.

2. Rough polish, 6 μm diamond with 6 parts alcohol and 1 part Gama-Medica Surgica Soap (Huntingdon Labs).

3. Final polish, 1 μm diamond with alcohol and soap.

4. Swab etch (20°C), equal parts nitric acid, hydroflouric acid and water.

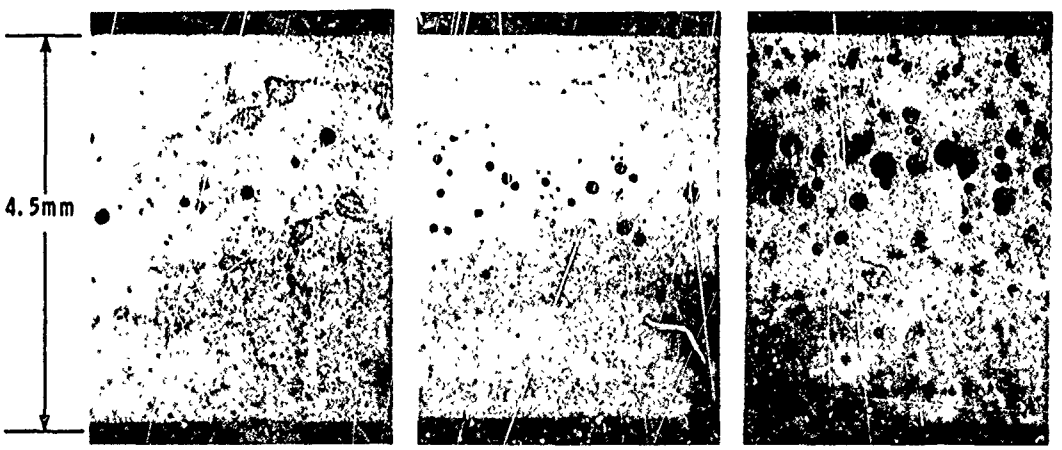

Figure 19 Spall Fractures in Tantalum (1.5 mm → 4.5 mm)

* All spall photomicrographs in this report are oriented such that initial shock wave propagation was from bottom to top.

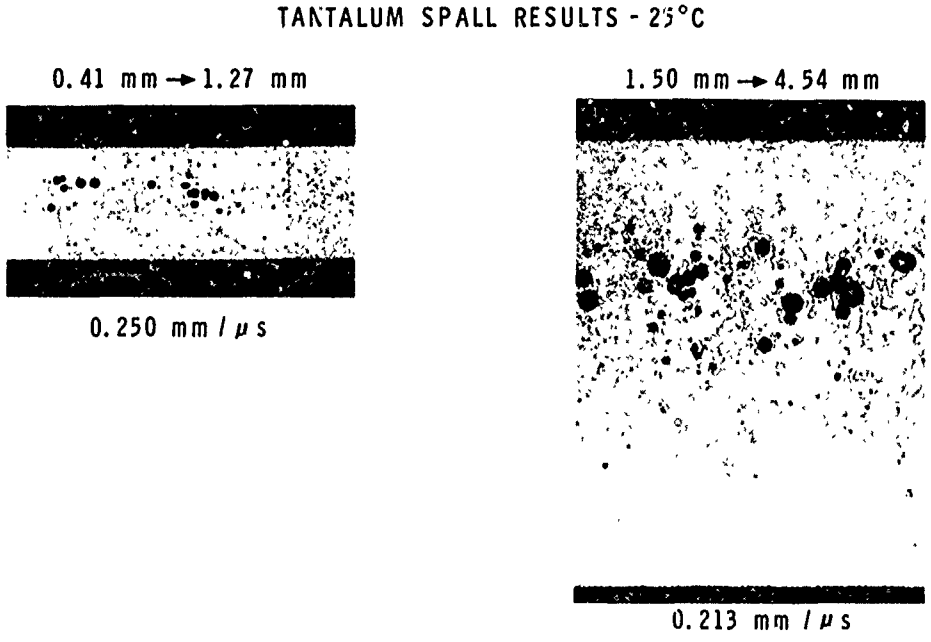

Figure 20 Spall Fractures in Tantalum

As noted above, spall cannot be rigorously defined in terms of a unique impact velocity or stress, but requires consideration of the degree of fracture. Fracture in tantalum is of a ductile nature with the development of spherical voids. As velocity increases (see Figure 19), the voids begin to coalesce and a complete fracture surface is formed. Note that there is dispersion of the voids around a nominal "spall plane". This was also found for 6061-T6 aluminum[50] and titanium[51], which have well-defined elastic wave structures, while copper[52] has a poorly defined, low amplitude elastic wave and showed very little void dispersion around the spall plane.

Scanning microfractographs of fracture surfaces for completely spalled specimens are given in Figures 21 and 22. Fracture was by normal rupture with evidence of extensive plastic flow. At -195°C, fracture is still ductile with no evidence of a ductile-brittle transition, but void size is much smaller.

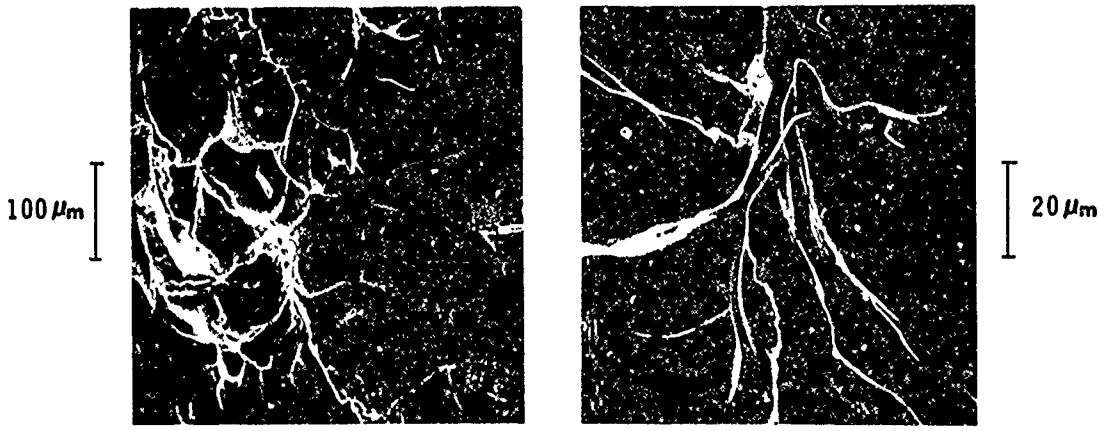

Figure 21 Spall Fracture Surfaces in Tantalum (1.5 mm → 4.5 mm, 0.32 mm/μs)

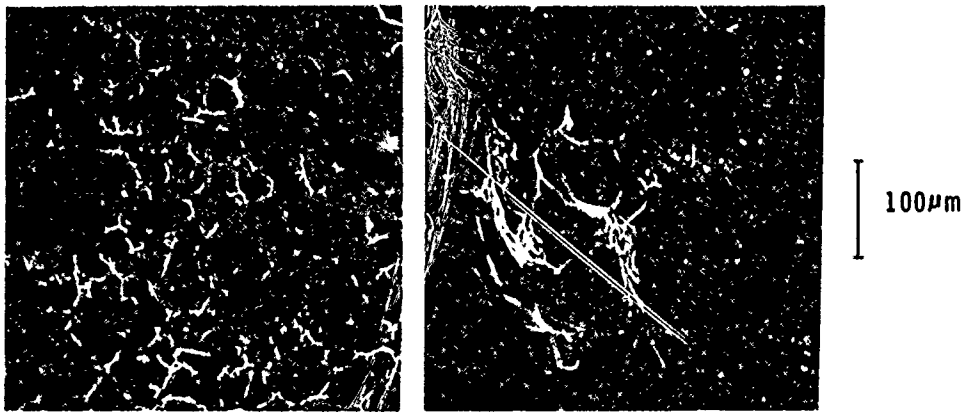

Figrue 22 Spall Fracture Surfaces in Tantalum, Temperature Effects

SPALL PROFILES

Complete wave profiles were obtained under spall-producing conditions using a tantalum-into-tantalum configuration, with a free rear surface on the impactor to give complete release and a free rear surface on the target for reflection of the compressive wave. The wave interactions resulting from such a test are discussed in Reference 53. Measured profiles for unattenuated pulses are given in Figure 23, with photomicrographs of the recovered and sectioned targets. Also shown for reference are the incipient and complete spall levels for this impactor/target combination as determined from recovery tests. Evidence of fracture is shown as reversal of the release wave. The amount of pullback (decrease in free surface velocity to the point of first reversal) may be related to spall strength of the material for a given impact geometry. An empirical relation for this has been given by Taylor[54] as:

$$\sigma_S = \rho C(\Delta u_{fs}/2) \qquad (23)$$

where σ_S is spall strength, ρ and C are local density and longitudinal wave speed, and Δu_{fs} is pullback.

The data in Figure 23 give $\sigma_S \simeq 68$ kbar. This calculated spall strength is not constant for a given material since it is proportional to Δu_{fs}. This factor has been found to change with target temperature, pulse width and pulse shape for 1-T6 aluminum,[53] and other metals such as tantalum may show similar behavior. A spall profile for polycrystalline tantalum reported by Taylor[54] showed a pullback of 0.12 mm/μsec for a pulse width of ∿ 1.5 μsec, which is less than the pullback of 0.19 mm/μsec shown in Figure 23 for a 0.8 μsec pulse

width. However, for a given set of impact conditions (X_o, X, temperature), the pullback is relatively insensitive to maximum compressive stress as well as to degree of fracture. The spall profile from an attenuated pulse test, where the impact velocity was above that required for spall, is given in Figure 24.

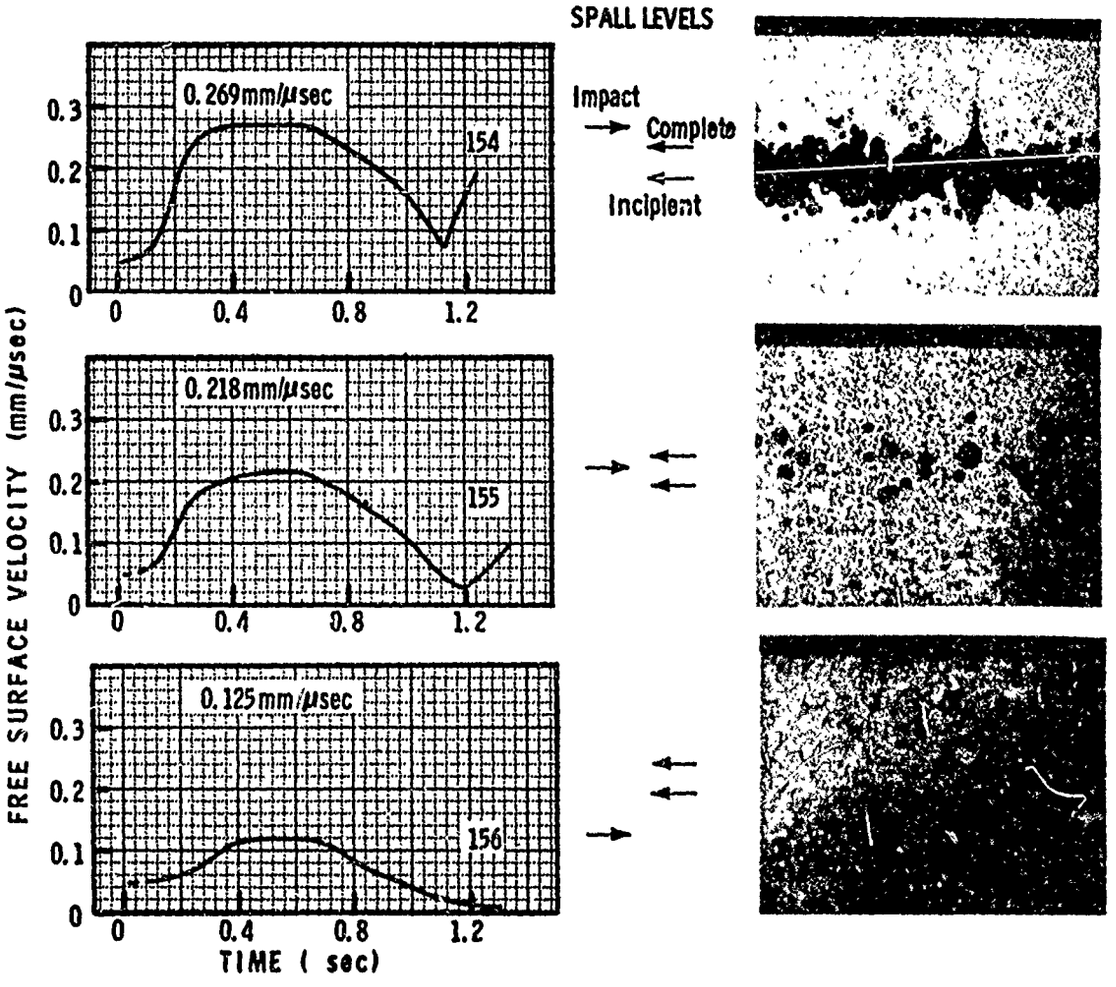

Figure 23 Spall Wave Profiles in Tantalum

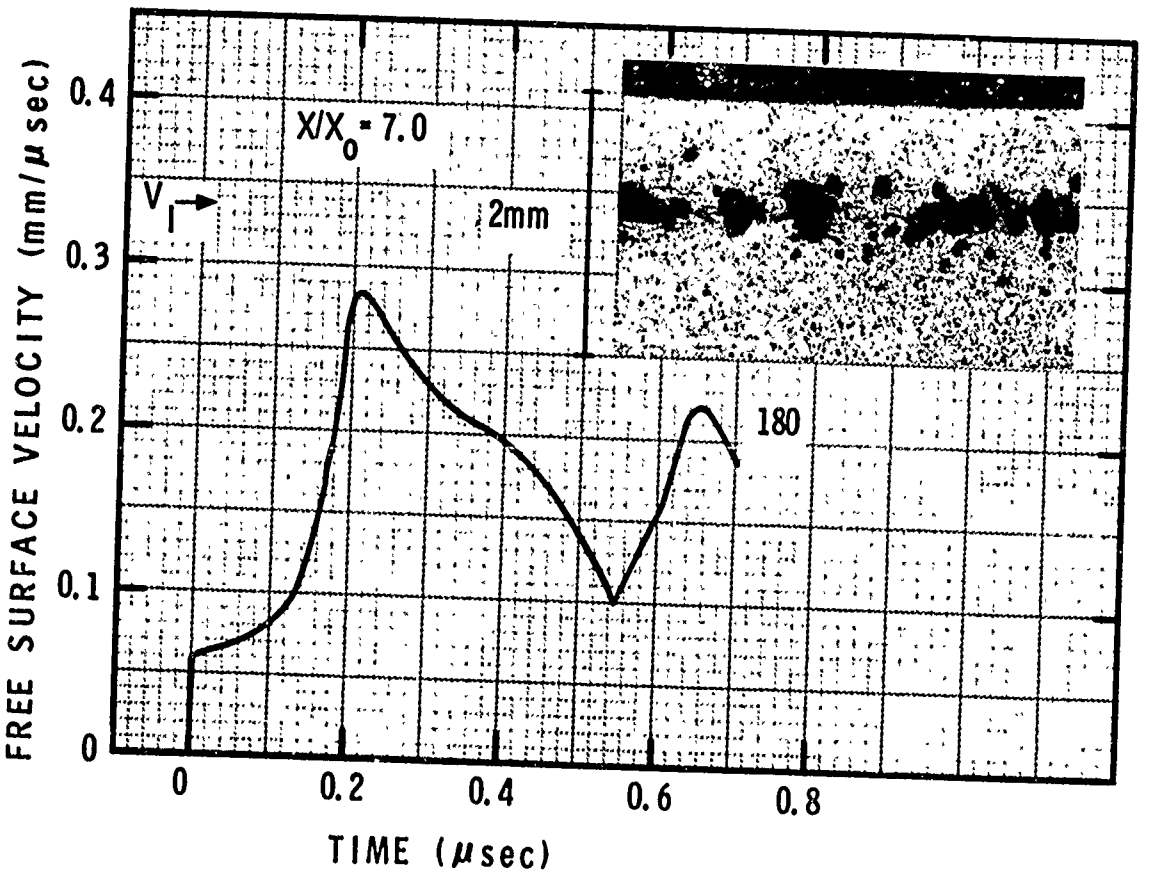

Figure 24 Attenuated Spall Profile in Tantalum

SUMMARY

The dynamic properties of tantalum were measured under uniaxial stress and uniaxial strain conditions. The material tested was commercially-pure bar stock with 45 to 500 μm grain size and 52 R_K hardness. Material response to compressive uniaxial strain deformation approximated elastic-perfectly plastic behavior and exhibited strain-rate sensitivity with ∿ 1.4 kbar yield at 0.001/sec and ∿ 5.4 kbar yield at 800/sec.

Longitudinal and shear wave velocities were measured as functions of temperature and pressure, giving the following (in mm/μsec):

$$C_L = 4.149 - 0.000146T$$

$$C_S = 2.036 - 0.000173T$$

(T in °C)

$$C_L = 4.146 + 0.00291P$$

$$C_S = 2.032 + 0.00137P$$

(P in kbar)

Principal elastic constants were evaluated at T = 20°C and P = 0, including:

Bulk Modulus = K_0^S = 1946 kbar

$$\left(\frac{\partial K^S}{\partial P}\right)_S = 3.77, \qquad \left(\frac{\partial K^S}{\partial P}\right)_T = 3.79$$

Shear Modulus = G_0^S = 688 kbar

$$\left(\frac{\partial G^S}{\partial P}\right)_S = 1.25, \qquad \left(\frac{\partial G^S}{\partial P}\right)_T = 1.28$$

Poisson's Ratio = 0.342

Elastic wave velocity data were also used in determining the Gruneisen parameter γ and the Debye temperature θ:

$\gamma = 1.63$ @ T = 20°C and P = 0

$$\frac{\partial \gamma}{\partial T} = -\ 0.00043/°C \text{ @ } T = 20°C$$

$$\frac{\partial \gamma}{\partial P} = -\ 0.00077/\text{kbar} \text{ @ } P = 0$$

$\theta = 260°K$

The shock wave hugoniot was determined experimentally to be:

$$\sigma_H = 4.0 + 550\ u_p + 215\ u_p^2 \qquad (\sigma_H < 200 \text{ kbar})$$

Assumption of an ideal elastic-plastic wave structure with a 20 kbar hugoniot elastic limit and equilibrium initial and final states gave:

$$\sigma_H = 7.2 + 1820\mu + 3120\mu^2$$

$$P_H = 1820\ \mu + 3120\ \mu^2$$

$$U_S = 3.36 + 1.239\ u_p$$

The hydrostat as determined from elastic constants data was:

$$P_H = 6063 \left[\left(1+\mu\right)^{1.10} - 1 \right] - 4723 \ln \left(1+\mu\right) + 1261 \left(\frac{\mu}{1+\mu}\right)^3$$

(Keane equation of state)

Measurements of compressive wave development showed the wave front to be characterized by a well-defined elastic portion and a transition to a spreading plastic wave. Elastic precursor decay was ∿ 50% to 19 kbar after 2 mm of travel.

Spall fracture behavior was determined for elastic pulse widths of 0.20 and 0.72 μsec. The incipient spall threshold expressed as impact velocity increased with decreasing pulse width. Tantalum showed a poorly-defined spall plane with appreciable dispersion of almost spherical voids. The fracture surface for completely spalled tantalum showed ductile failure with void growth and coalescence accompanied by a large amount of plastic flow.

ACKNOWLEDGMENTS

The assistance of the following Materials and Structures Laboratory personnel in the experimental work is gratefully recognized: Mr. B. Bielski and Mr. J. Wigton for specimen preparation; Mr. F. Stemczynski and Mr. E. Miller for EOS and wave profile tests; Mr. J. Havens for ultrasonics measurements; Mr. C. Woodcock for spall tests; Mr. J. Bonner and Mr. H. Simmons for strain rate tests; Mr. C. Whitchurch and Mr. L. Seltz for metallographic work; and Mrs. C. Strong for data analysis.

REFERENCES

1. "A Selected Bibliography on Dynamic Properties of Materials", compiled by Christman, D. R., General Motors Corporation, Manufacturing Development, DASA 2511, June, 1970 (AD 710823).

2. Metals Handbook, 8th Ed., Vol. 1: Properties and Selection of Metals, Lyman, T., Ed., American Society for Metals, Metals Park, Ohio, 1961.

3. Handbook of Chemistry and Physics, 45th Ed., Weast, R. C., Ed., The Chemical Rubber Co., Cleveland, Ohio, 1964.

4. Thermophysical Properties of High Temperature Solid Materials, Vol. 1: Elements, Touloukian, Y. S., Ed., The McMillan Co., New York, N. Y., 1967.

5. Aerospace Structural Metals Handbook, Chapter Code 5401 (Tantalum), Mechanical Properties Data Center, Belfour Stulen, Inc., Traverse City, Michigan, 1966.

6. Pink, E., "Zum Einfluss der Dehngeschwindigkeit auf Streckgrenzen Phanomene bei Tantal", J. Less-Common Metals, Vol. 16, p. 119-128, 1969.

7. Hoge, K. G., "Influence of Strain Rate on Flow Stress of Tantalum", Proc. Second Int. Conf. Strength of Metals and Alloys, Vol. III, American Society for Metals, p. 996-1000, 1970.

8. Arsenault, R. J., "Effects of Strain Rate and Temperature on Yield Points", AIME Trans., Vol. 230, p. 1570-1576, 1964.

9. Hoge, K. G., "The Effect of Strain Rate on Mechanical Properties of Some Widely Used Engineering Metals", University of California Radiation Laboratory, UCRL-14599, 14 Dec. 1965.

10. Kossowsky, R., "Temperature and Strain Rate Dependence of Microyield Points in Tantalum", Refractory Metals and Alloys IV: Vol. I, Vol. 41, Met. Soc. Conf., Gordon and Breach, New York, N. Y., p. 47-68, 1967.

11. Barbee, T. W. and Huggins, R. A., "Dislocation Structures in Deformed and Recovered Tantalum", Stanford University, ONRDMS Report No. 64-25, Nov., 1964.

12. Nunes, J., Anctil, A. A. and Kula, E. B., "Low Temperature Flow and Fracture Behavior of Tantalum", U.S. Army Materials Research Agency, AMRA-TR-64-22, Aug., 1964 (AD 448479).

13. Arsenault, R. J., "An Investigation of the Mechanism of Thermally Activated Deformation in Tantalum and Tantalum-Base Alloys", Acta Met., Vol. 14, p. 831-838, 1966.

14. Gazza, G. E., "Petch Analysis of Hydrogenated Tantalum Sheet", Refractory Metals and Alloys IV: Vol. I, Vol. 41, Met. Soc. Conf., Gordon and Breach, New York, N. Y., p. 69-80, 1967 (also, AD 635596).

15. Eliasz, W. and Szkopiak, Z. C., "Strain Aging of Refractory Metals (Tantalum)", Air Force Materials Laboratory, AFML-TR-65-437, July, 1965 (AD 808649).

16. Owen, W. S., Hull, D. C., Bryson, J. and Formby, C. L., "Plastic Deformation of Body-Centered Cubic Metals, Vol. I: Plastic Deformation of Tantalum", University of Liverpool, AFML-TR-66-369, Vol. I, Feb., 1967 (AD 813542).

17. Barbee, T. W., "Some Aspects of Dislocation Dynamics in Metals...", Stanford University, ONR SU-DMS Report No. 65-33, Nov., 1965 (AD 625023).

18. Jewett, R. P. and Weisert, E. D., "Dislocation Morphology of Tantalum Deformed in Tension", High Temperature Refractory Metals, Vol. 34, Met. Soc. Conf., Gordon and Breach, New York, N. Y., p. 160-172, 1966.

19. Hoddinott, D. S. and Davies, G. J., "The Anisotropy of Young's Modulus and Texture in Sheets of B.C.C. Metals", J. Inst. Met., Vol. 97, p. 155-159, 1969.

20. Soga, N., "Comparison of Measured and Predicted Bulk Moduli of Tantalum and Tungsten at High Temperatures", J. Appl. Phys., Vol. 37, p. 3416-3420, 1966.

21. Chechile, R. A., "Ultrasonic Equati of State of Tantalum", Case Institute of Technology, May, 1967 (AD 655640).

22. Palmieri, L., "Ultrasonic Measurements of Elastic Moduli of Polycrystalline Tantalum and Niobium", Appl. Mat. Res., Vol. 3, p. 139-143, 1964.

23. Armstrong, P. E. and Brown, H. L., "Dynamic Young's Modulus Measurements Above 1000°C on Some Pure Polycrystalline Metals and Commerical Graphites", AIME Trans., Vol. 230, p. 962-966, 1964.

24. Lamberson, D. L., "The High Pressure Equation of State of Tantalum, Polystyrene and Carbon Phenolic Determined from Ultrasonic Velocities", Doctoral Dissertation, Air Force Institute of Technology (AFIT-SE), Wright-Patterson AFB, Ohio, March, 1969.

25. Bolef, D. I., "Elastic Constants of Single Crystals of the bcc Transition Elements V, Nb, and Ta", J. Appl. Phys., Vol. 32, p. 100-105, 1961.

26. Featherston, F. H. and Neighbours, J. R., "Elastic Constants of Tantalum, Tungsten, and Molybdenum", Phys. Rev., Vol. 130, p. 1324-1333, 1963.

27. Rice, M. H., McQueen, R. G. and Walsh, J. M., "Compression of Solids by Strong Shock Waves", Solid State Physics, Vol. 6, p. 1-63, 1958.

28. Slater, J. C., Introduction to Chemical Physics, McGraw-Hill Book Co., New York, N. Y., 1939.

29. Dugdale, J. S. and MacDonald, D. K. C., "The Thermal Expansion of Solids", Phys. Rev., Vol. 89, p. 832-834, 1953.

30. Schreiber, E. and Anderson, O. L., "Pressure Derivatives of the Sound Velocities of Polycrystalline Alumina", Am. Ceram. Soc. J., Vol. 49, p. 184-190, 1966.

31. Anderson, O. L. and Dienes, G. J., Non-Crystalline Solids (Chapter 18), Ed. by Frechette, V. D., John Wiley and Sons, New York, 1960.

32. Schuele, D. E. and Smith, C. S., "Low Temperature Thermal Expansion of RbI", J. Phys. Chem. Solids, Vol. 25, p. 801-814, 1964.

33. Alers, G. A., "Use of Sound Velocity Measurements in Determining the Debye Temperature of Solids", Physical Acoustics, Vol. III, Part B (Lattice Dynamics), Academic Press, New York, N. Y., p. 1-42, 1965.

34. Taylor, A. and Kagle, B. J., Crystallographic Data on Metal and Alloy Structures, Dover Publications, Inc., New York, N. Y., 1963.

35. Chin, H. C., "A Computer Program to Analyze X-Cut Quartz Data Obtained from Shock Loading", General Motors Corporation, Manufacturing Development, Materials and Structures Laboratory, MSL-70-15, June, 1970.

36. Group GMX-6, "Selected Hugoniots", Los Alamos Scientific Laboratory, LA-4167-MS, 1 May 1969.

37. Rohde, R. W. and Towne, T. L., "Shock-Compression Behavior of Tantalum at 25° and 900°C", J. Appl. Phys., Vol. 42, p. 878-880, 1971.

38. Birch, F., "The Effect of Pressure Upon the Elastic Parameters of Isotropic Solids, According to Murnaghan's Theory of Finite Strain", J. Appl. Phys., Vol. 9, p. 279-288, 1938.

39. Birch, F., "Elasticity and Constitution of the Earth's Interior", J. Geophys. Res., Vol. 57, p. 227-286, 1952.

40. Murnaghan, F. D., "The Compressibility of Media Under Extreme Pressures", Proc. Nat. Ac. Sci., Vol. 30, p. 244-247, 1944.

41. Keane, A., "An Investigation of Finite Strain in an Isotropic Material Subjected to Hydrostatic Presssure and Its Seismological Applications", Australian J. Phys., Vol. 7, p. 323-333, 1954.

42. Anderson, O. L., "On the Use of Ultrasonic and Shock-Wave Data to Estimate Compressions at Extremely High Pressures", Phys. Earth Planet. Interiors, Vol. 1, p. 169-176, 1968.

43. Duvall, G. E. and Zwolinski, B. J., "Entropic Equations of State and Their Applications to Shock Wave Phenomena in Solids", Acoust. Soc. Am., Vol. 27, p. 1054-1058, 1955.

44. Zel'dovich, Y. B and Raizer, Y. P., Physics of Shock Waves and High-Temperature Hydrodynamic Phenomena, Vol. II, Academic Press, New York, N. Y., p. 688-709, 1967.

45. Ruoff, A. L., "Linear Shock-Velocity-Particle-Velocity Relationship", J. Appl. Phys., Vol. 38, p. 4976-4980, 1967.

46. Vaidya, S. N. and Kennedy, G. C., "Compressibility of 18 Metals to 45 kbar", J. Phys. Chem. Solids, Vol. 31, p. 2329-2345, 1970.

47. Gillis, P. P., Hoge, K. G. and Wasley, R. J., "Elastic Precursor Decay in Tantalum", J. Appl. Phys., Vol. 42, p. 2145-2146, 1971.

48. Barker, L. M. and Hollenbach, R. E., "Shock-Wave Studies of PMMA, Fused Silica and Sapphire", J. Appl. Phys., Vol. 41, p. 4208-4226, 1970.

49. Hanneman, G. P., "Spallation Threshold Tests on Niobium, Tantalum and Zirconium", Battelle Northwest Laboratories, BNWL-756, Sept., 1968.

50. Christman, D. R., Isbell, W. M., Babcock, S. G., McMillan, A. R. and Green, S. J., "Measurements of Dynamic Properties of Materials, Vol. III: 6061-T6 Aluminum", General Motors Corporation, Manufacturing Development, DASA 2501-3, 1971.

51. Christman, D. R., Michaels, T. E., Isbell, W. M. and Babcock, S. G., "Measurements of Dynamic Properties of Materials, Vol. IV: Alpha Titanium", General Motors Corporation, Manufacturing Development, DASA 2501-4, 1971.

52. Christman, D. R., Isbell, W. M. and Babcock, S. G., "Measurements of Dynamic Properties of Materials, Vol. V: OFHC Copper", General Motors Corporation, Manufacturing Development, DASA 2501-5, July, 1971 (AD 728846).

53. Isbell, W. M. and Christman, D. R., "Shock Propagation and Fracture in 6061-T6 Aluminum from Wave Profile Measurements", General Motors Corporation, Manufacturing Development, DASA 2419, April, 1970 (AD 705536).

54. Taylor, J. W., "Stress Wave Profiles in Several Metals", Dislocation Dynamics, p. 573-589, McGraw-Hill Book Co., New York, N. Y., 1968.

APPENDIX A

GRUNEISEN PARAMETER ESTIMATES

1. The Gruneisen parameter is expressed thermodynamically as

$$\gamma = -\frac{1}{\rho c_p}\left(\frac{\partial V}{\partial T}\right)_P \left(\frac{\partial P}{\partial V}\right)_S = \frac{\beta K^S}{\rho c_p}$$

For an isotropic elastic solid, this becomes

$$\gamma = \frac{\beta}{c_p}\left(C_L^2 - \frac{4}{3} C_S^2\right)$$

Substituting appropriate values for tantalum gives

$$\gamma_0 = 1.63$$

2. Slater developed a relation that was an extension of the Debye Theory for a three-dimensional continuum, and assumed Poisson's ratio was independent of volume and γ is the same for all vibrational frequencies:

$$\gamma = -\frac{V}{2}\left(\frac{\partial^2 P/\partial V^2}{\partial P/\partial V}\right) - \frac{2}{3}$$

which simplifies at zero pressure to

$$\gamma_0 = \frac{1}{2}\left(K_{0S}^{S'} - \frac{1}{3}\right) = 2S - \frac{2}{3}$$

where S is from $U_S = C_B + Su_p$.

Ultrasonic data gives S = 1.193 and γ = 1.72.

Shock wave data gives S = 1.239 and γ = 1.81.

3. Dugdale and MacDonald give an expression for plane wave velocity vs. volume in a three-dimensional continuum that leads to an expression for γ differing from Slater's by a constant (1/3):

$$\gamma = -\frac{V}{2}\left(\frac{\partial^2 P/\partial V^2}{\partial P/\partial V}\right) - 1$$

which simplifies at zero pressure to

$$\gamma_0 = \frac{1}{2}\left(K_{0S}^{S'} - 1\right) = 2S - 1$$

From ultrasonic data, γ = 1.39.

From shock wave data, γ = 1.48.

4. Anderson and Dienes give expressions for γ in terms of the longitudinal and shear modes of wave propagation:

$$\gamma_L = \frac{1}{3} + \frac{K_0^T}{C_L} \left(\frac{dC_L}{dP}\right)_0$$

$$\gamma_S = \frac{1}{3} + \frac{K_0^T}{C_S} \left(\frac{dC_S}{dP}\right)_0$$

Ultrasonic data gives $\gamma_L = 1.69$ and $\gamma_S = 1.63$.

5. Schuele and Smith give expressions for the "low-temperature" and "high-temperature" Grueisen ratio, where low-temperature is the range in which it is assumed the solid behaves as a continuum and high-temperature is the range where all vibrational modes are excited and γ is constant:

$$\gamma_{LT} = \frac{1}{2+\varepsilon^3} \left(\varepsilon^3 \gamma_L + 2\gamma_S\right)$$

$$(\varepsilon = C_S/C_L)$$

$$\gamma_{HT} = \frac{1}{3} \left(\gamma_L + 2\gamma_S\right)$$

Using ultrasonic data and γ_L and γ_S from above gives $\gamma_{LT} = 1.63$ and $\gamma_{HT} = 1.65$.

6. Perry calculated the Grueisen parameter from laser interferometer data obtained for electron beam energy deposition.* for polycrystalline tantalum, he obtained $\gamma = 0.95$ assuming instantaneous deposition and $\gamma = 1.60$ assuming 50 nsec deposition time.

(All ultrasonics data used in this Appendix are for zero pressure and 20°C).

* Perry, F. C., "Thermoelastic Response of Polycrystalline Metals to Relativistic Electron Beam Absorption", J. Appl. Phys., Vol. 41, p. 5017-5022, 1970.

APPENDIX B

DEVIATORIC STRESS ESTIMATES

The shock wave equation of state for tantalum is given by:

$$\left.\begin{aligned} \sigma_H &= 4.0 + 550\ u_p + 215\ u_p^2 \\ \sigma_H &= 7.2 + 1820\ \mu + 3120\ \mu^2 \\ P_H &= 1820\ \mu + 3120\ \mu^2 \text{ (Hydrostat)} \end{aligned}\right\} \qquad \text{(B-1)}$$

where $\mu = (v_o/v) - 1.$

The deviatoric stress (σ_D) can be defined as the difference between the dynamic stress-compression path (σ_H - μ) and the hydrostat, and is a measure of the material's ability to support shear. If the material strain hardens, the deviatoric stress will be a function of μ. In Equation B-1, σ_D was assumed constant at 7.2 kbar which gives $P_H = \sigma_H - 7.2$.

The deviatoric stress can also be estimated from uniaxial stress data, shock wave data or ultrasonics data as follows:

$$\sigma_D = \sigma_H - P_H = \frac{2}{3} Y \qquad \text{(B-2)}$$

where Y is flow stress under uniaxial stress conditions.

A. The flow stress at low strain rate from the uniaxial stress tests (see Figure 3) is ∿2 kbar, which gives σ_D = 1.3 kbar.

B. For a hugoniot elastic limit (σ_e) of 20 kbar, the relation $Y = \sigma_e (1-2\nu/1-\nu)$ gives Y = 9.6 kbar. From Equation B-2, σ_D = 6.4 kbar.

C. Since σ_D can also be taken as the difference between σ_H and P_H at a compression corresponding to the hugoniot elastic limit, one has

$$\sigma_D = \sigma_H - P_H = \sigma_e - P_e$$

where

$$\sigma_e = \rho_0 C_L^2 \left(\frac{\mu_e}{1+\mu_e}\right) = 2864 \left(\frac{\mu_e}{1+\mu_e}\right)$$

$$P_e = \rho_0 C_B^2 \left(\frac{\mu_e}{1+\mu_e}\right) = 1949 \left(\frac{\mu_e}{1+\mu_e}\right)$$

For σ_e = 20 kbar: μ_e = 0.007 and P_e = 13.5 kbar. This gives σ_D = 6.5 kbar.

The estimates from B and C, above, agree reasonably well with the value of 7.2 kbar from Equation B-1, considering the assumptions underlying each method and the experimental inaccuracies. The estimate from A, however, is significantly lower, which may be a consequence of the high strain rate sensitivity of tantalum.

Also, it should be noted that the stress-axis intercept is larger in the σ_H - μ plane than the σ_H - u_p plane. Assuming linear elastic and hydrostatic behavior up to the elastic limit, then:

σ_H - u_p plane -

$$\sigma_{D_u} = \rho_0 u_e (C_L - C_B)$$

σ_H - μ plane -

$$\sigma_{D_\mu} = \frac{\mu_e}{1+\mu_e} \left(\rho_0 C_L^2 - \rho_0 C_B^2 \right)$$

Using the approximations $u_e \simeq \mu_e / C_L$ and $\mu_e \simeq \mu_e / (1+\mu_e)$, and subtracting:

$$\Delta\sigma_D = \sigma_{D_u} - \sigma_{D_\mu} = \rho_0 C_B \mu_e (C_L - C_B)$$

For σ_e = 20 kbar, μ_e = 0.007 and $\Delta\sigma_D$ = 2.9 kbar, compared to $\Delta\sigma_D$ = 3.2 kbar from σ_H - u_p and σ_H - μ given in Equation B-1.

APPENDIX C

EQUATIONS OF STATE, ULTRASONIC

Numerous analytical and empirical relations have been developed for determining equations of state from ultrasonics data. Some of these are presented here.

1. The Birch equation of state for the isotherm can be expressed as:*

$$P_T = \frac{3}{2} K_0^T \left[\left(1+\mu\right)^{7/3} - \left(1+\mu\right)^{5/3} \right] \left[1-\xi \left\{ \left(1+\mu\right)^{2/3} - 1 \right\} \right]$$

where $\xi = \dfrac{12-3\ K_{0T}^{T'}}{4}$

$$P_T = 2891 \left[\left(1+\mu\right)^{7/3} - \left(1+\mu\right)^{5/3} \right] \left[1-0.15 \left\{ \left(1+\mu\right)^{2/3} - 1 \right\} \right]$$

---

* Another parameter sometimes used with this equation of state is

$$\alpha \left[(1+\mu)^{2/3} - 1 \right]^2$$

where $\alpha = \dfrac{3}{8} \left[K_0^T K_{0T}^{T''} - 7K_{0T}^{T'} + \left(K_{0T}^{T'} \right)^2 + \dfrac{143}{9} \right]$

However, this term can usually be neglected, contributing <0.4% at 100 kbar for tantalum.

2. The Murnaghan equation of state is derived by assuming the bulk modulus is linear with pressure which gives:

$$\text{Isotherm - } P_T = \frac{K_0^T}{K_{0T}^{T'}} \left[\left(1+\mu\right)^{K_{0T}^{T'}} - 1 \right]$$

$$P_T = 507.1 \left[\left(1+\mu\right)^{3.80} - 1 \right]$$

$$\text{Adiabat - } P_S = \frac{K_0^S}{K_{0S}^{S'}} \left[\left(1+\mu\right)^{K_{0S}^{S'}} - 1 \right]$$

$$P_S = 516.2 \left[\left(1+\mu\right)^{3.77} - 1 \right]$$

3. Instead of a linear bulk modulus-pressure relation, Keane assumed:

$$dK^S = \left[\frac{\left(K_0^{S'} - K_\infty^{S'} \right) K_0^S}{K^S} + K_\infty^{S'} \right] dP$$

where $K_\infty^{S'}$ is the limiting value of $K^{S'}$ at very high pressure.

This leads to:

$$P_S = \frac{K_0^S K_{0S}^{S'}}{\left(K_\infty^{S'} \right)^2} \left[\left(1+\mu\right)^{K_\infty^{S'}} - 1 \right] - \frac{\left(K_{0S}^{S'} - K_\infty^{S'} \right) K_0^S}{K_\infty^{S'}} \ln \left(1+\mu\right)$$

Anderson[42] suggested that this equation be applied by empirically determining $K_\infty^{S'}$. This can be done by evaluating the equation at a known high pressure shock wave point, i.e., the equation is solved for $K_\infty^{S'}$ at a known P_S, μ point. A high pressure data point was obtained by Shipman* at P_H = 1863 kbar and μ = 0.497. This value of P_H corresponds to P_S = 1817 kbar, using the entropy correction term suggested by Duvall[43] for the Murnaghan equation. Solving the above equation for $K_\infty^{S'}$ at P_S = 1817 kbar and μ = 0.497 gives

$$K_\infty^{S'} = 3.6$$

$$\therefore \quad P_S = 566.1 \left[\left(1+\mu\right)^{3.6} - 1 \right] - 91.9 \ln \left(1+\mu\right)$$

Huang** gives the upper bound for $K^{S'}$ as:

$$K_\infty^{S'} = 4S - \frac{11}{3} = K_{0S}^{S'} - \frac{8}{3} = 1.10$$

This gives:

$$P_S = 6063 \left[\left(1+\mu\right)^{1.10} - 1 \right] - 4723 \ln \left(1+\mu\right)$$

---

* Shipman, F. H., Unpublished Data, General Motors Corporation, May, 1971.

** Huang, Y. K., "Analytical Approach to the Shock Compressibility of 18 Cubic-Lattice Metals", J. Chem. Phys., Vol. 53, p. 571-575, 1970.

APPENDIX D

WAVE PROFILES

(Quartz Gage and Velocity Interferometer)

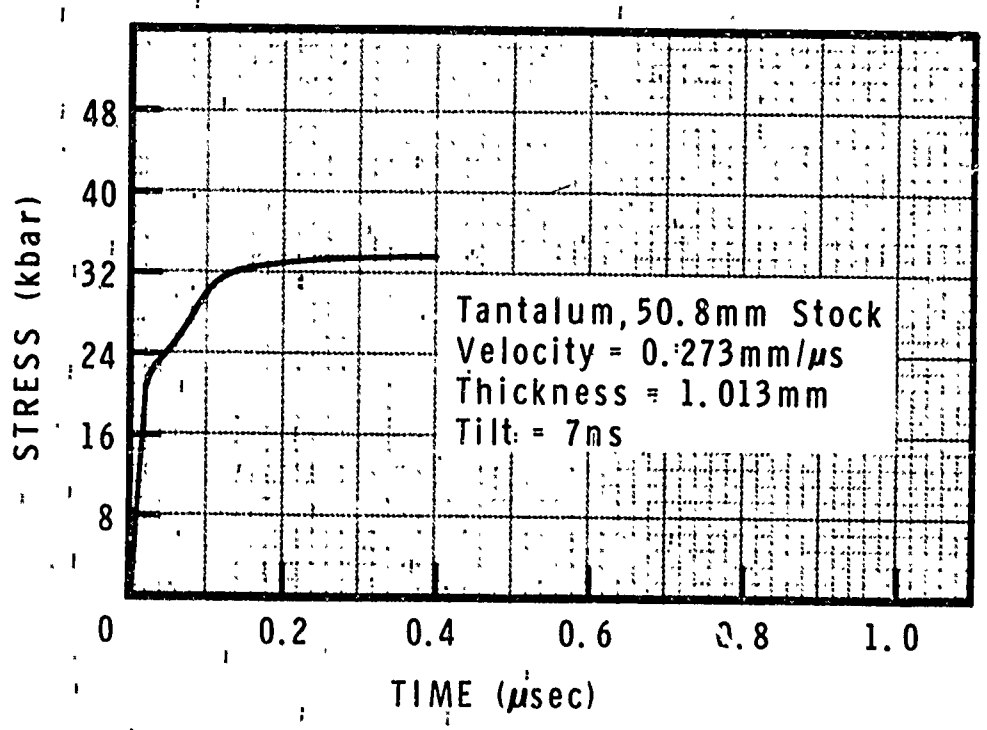
STRESS (kbar)
48
40
32
24
16
8
0
0.2
0.4
0.6
0.8
1.0
TIME (μsec)
Tantalum, 50.8mm Stock
Velocity = 0.273mm/μs
Thickness = 1.013mm
Tilt = 7ns

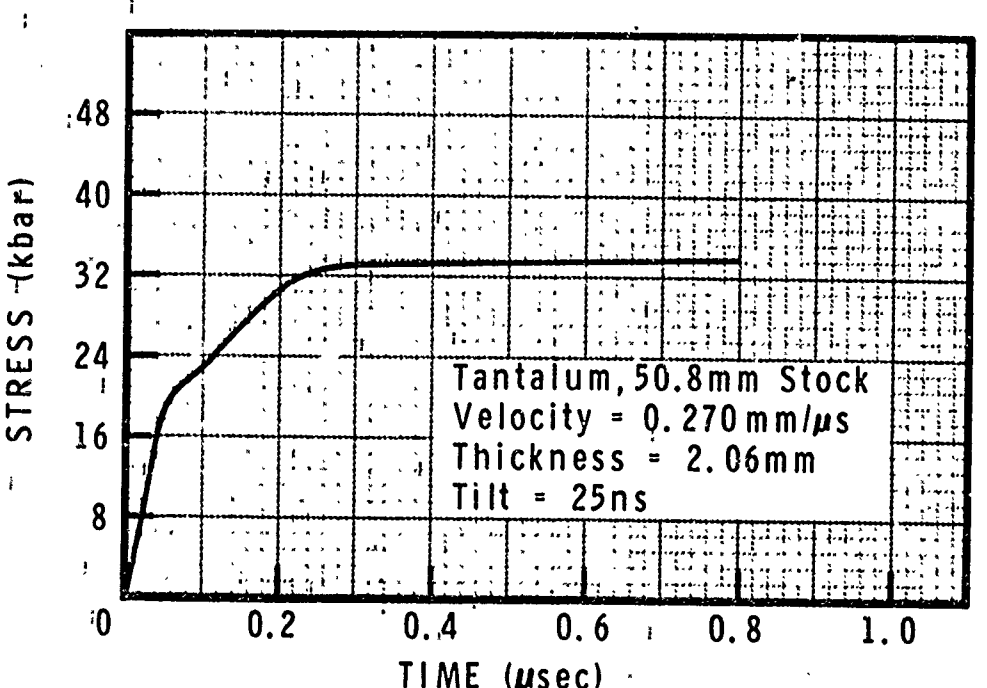
STRESS (kbar)
48
40
32
24
16
8
0
0.2
0.4
0.6
0.8
1.0
TIME (μsec)
Tantalum, 50.8mm Stock
Velocity = 0.270mm/μs
Thickness = 2.06mm
Tilt = 25ns

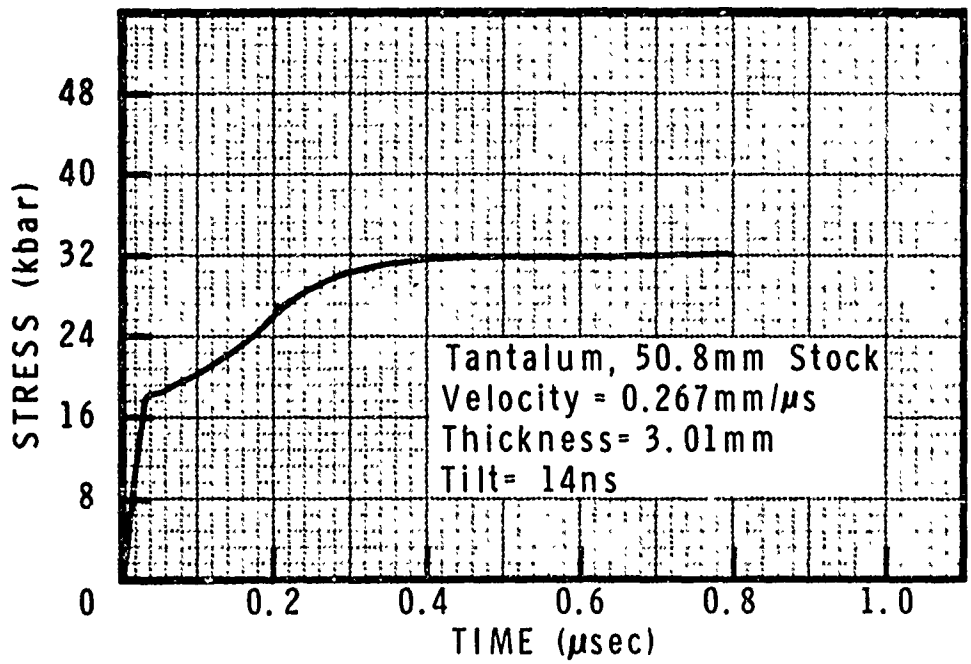
STRESS (kbar)
48
40
32
24
16
8
0
0.2
0.4
0.6
0.8
1.0
TIME (μsec)
Tantalum, 50.8mm Stock
Velocity = 0.267mm/μs
Thickness= 3.01mm
Tilt= 14ns

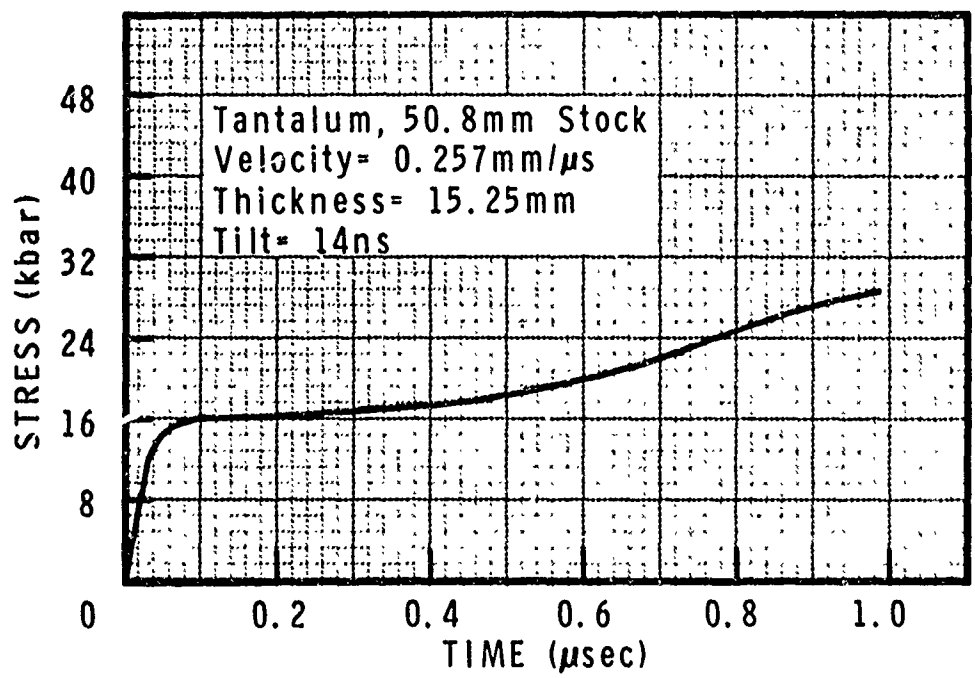
STRESS (kbar)
48
40
32
24
16
8
0
0.2
0.4
0.6
0.8
1.0
TIME (μsec)
Tantalum, 50.8mm Stock
Velocity= 0.257mm/μs
Thickness= 15.25mm
Tilt= 14ns

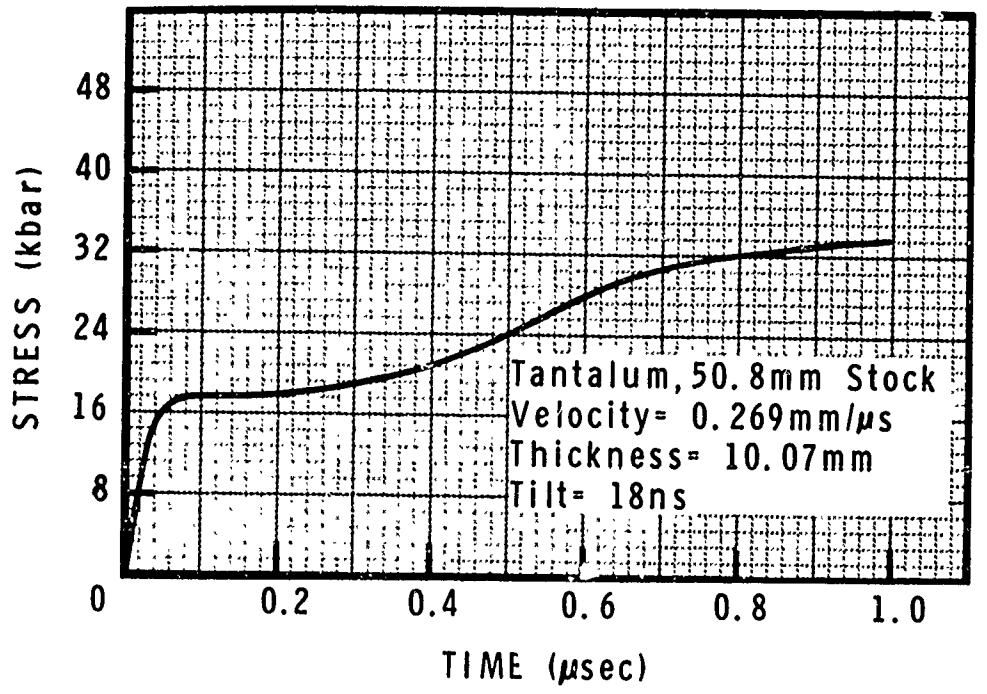
STRESS (kbar)
48
40
32
24
16
8
0
0.2
0.4
0.6
0.8
1.0
TIME (μsec)
Tantalum, 50.8mm Stock
Velocity= 0.269mm/μs
Thickness= 10.07mm
Tilt= 18ns

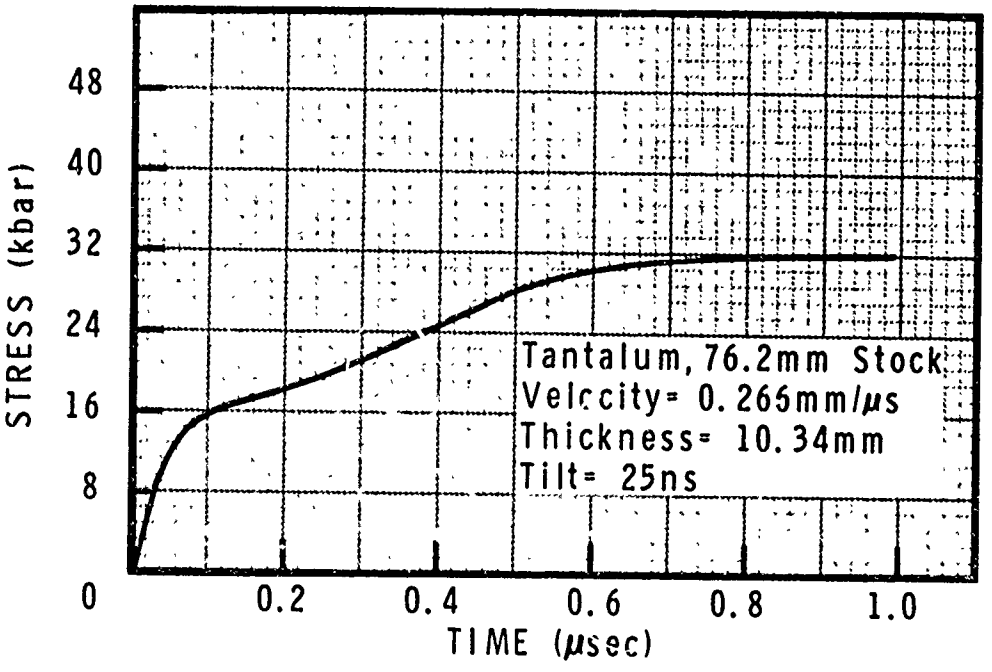
STRESS (kbar)
48
40
32
24
16
8
0
0.2
0.4
0.6
0.8
1.0
TIME (μsec)
Tantalum, 76.2mm Stock
Velocity= 0.266mm/μs
Thickness= 10.34mm
Tilt= 25ns

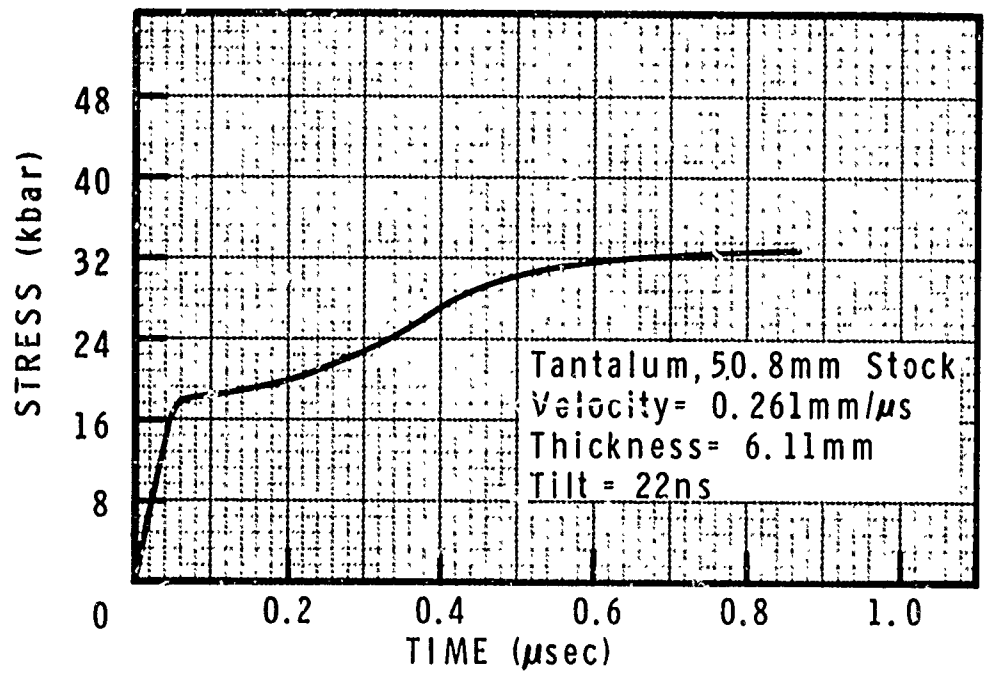
STRESS (kbar)
48
40
32
24
16
8
0
0.2
0.4
0.6
0.8
1.0
TIME (μsec)
Tantalum, 50.8mm Stock
Velocity= 0.261mm/μs
Thickness= 6.11mm
Tilt = 22ns

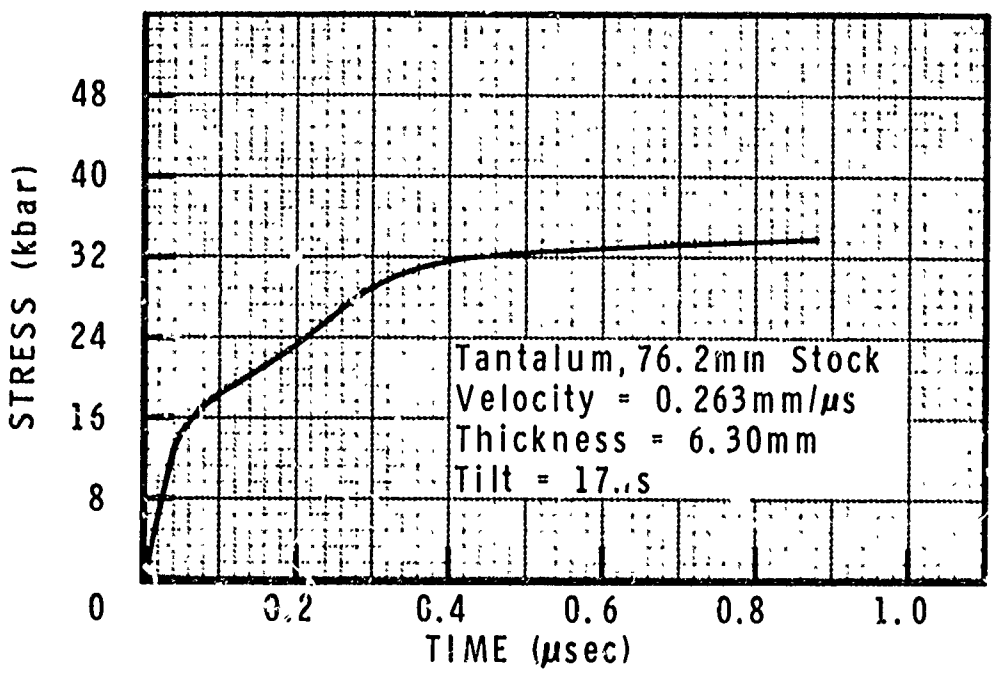
STRESS (kbar)
48
40
32
24
16
8
0
0.2
0.4
0.6
0.8
1.0
TIME (μsec)
Tantalum, 76.2mm Stock
Velocity = 0.263mm/μs
Thickness = 6.30mm
Tilt = 17.s

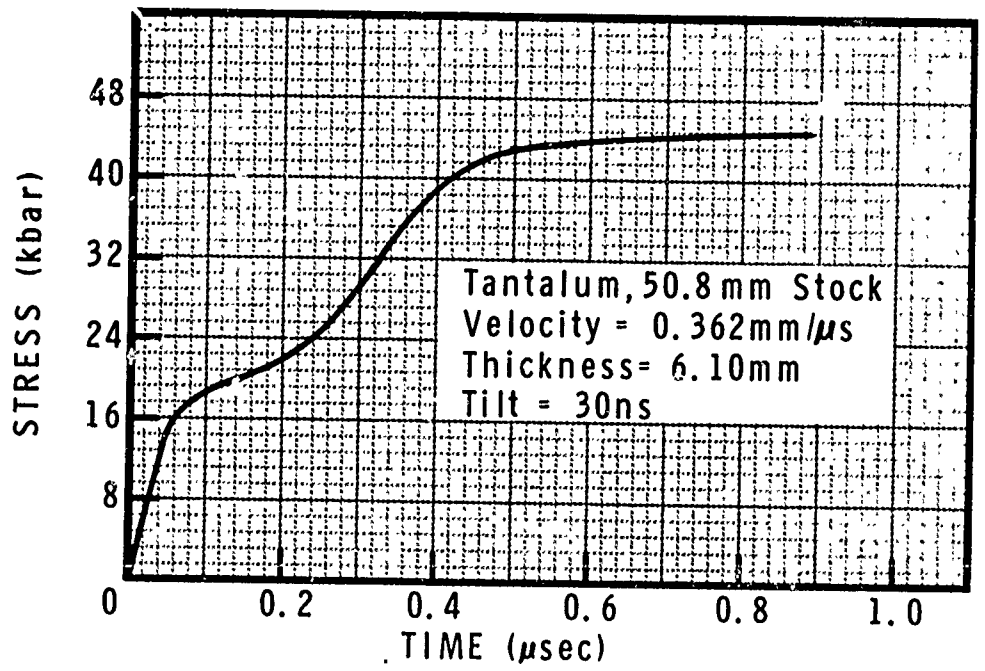
STRESS (kbar)
48
40
32
24
16
8
0
0.2
0.4
0.6
0.8
1.0
TIME (μsec)
Tantalum, 50.8 mm Stock
Velocity = 0.362mm/μs
Thickness= 6.10mm
Tilt = 30ns

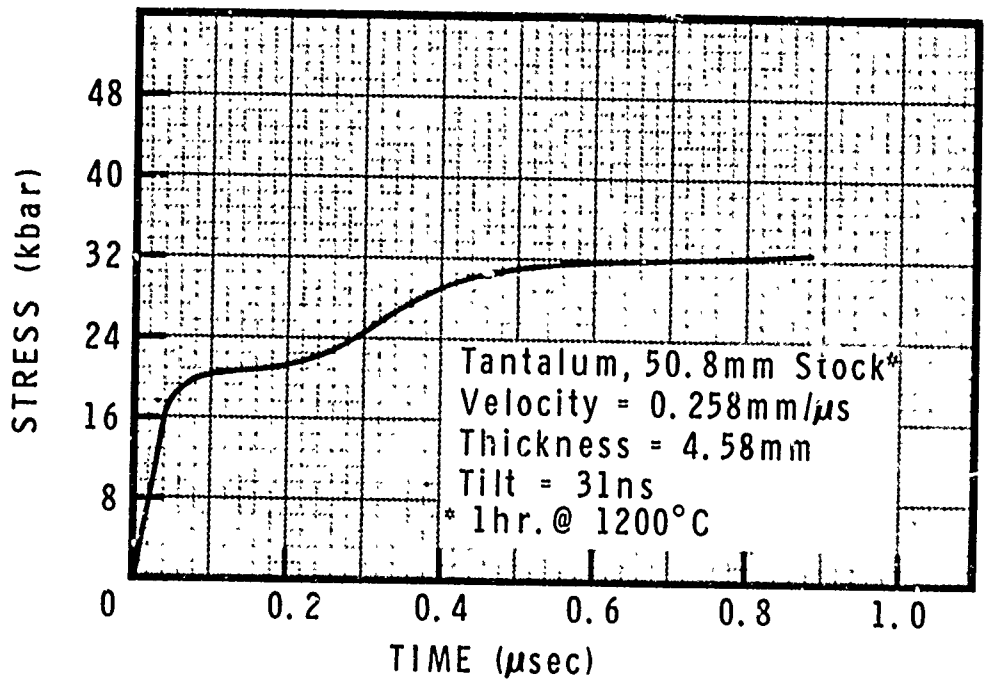
STRESS (kbar)
48
40
32
24
16
8
0
0.2
0.4
0.6
0.8
1.0
TIME (μsec)
Tantalum, 50.8mm Stock*
Velocity = 0.258mm/μs
Thickness = 4.58mm
Tilt = 31ns
* 1hr. @ 1200°C

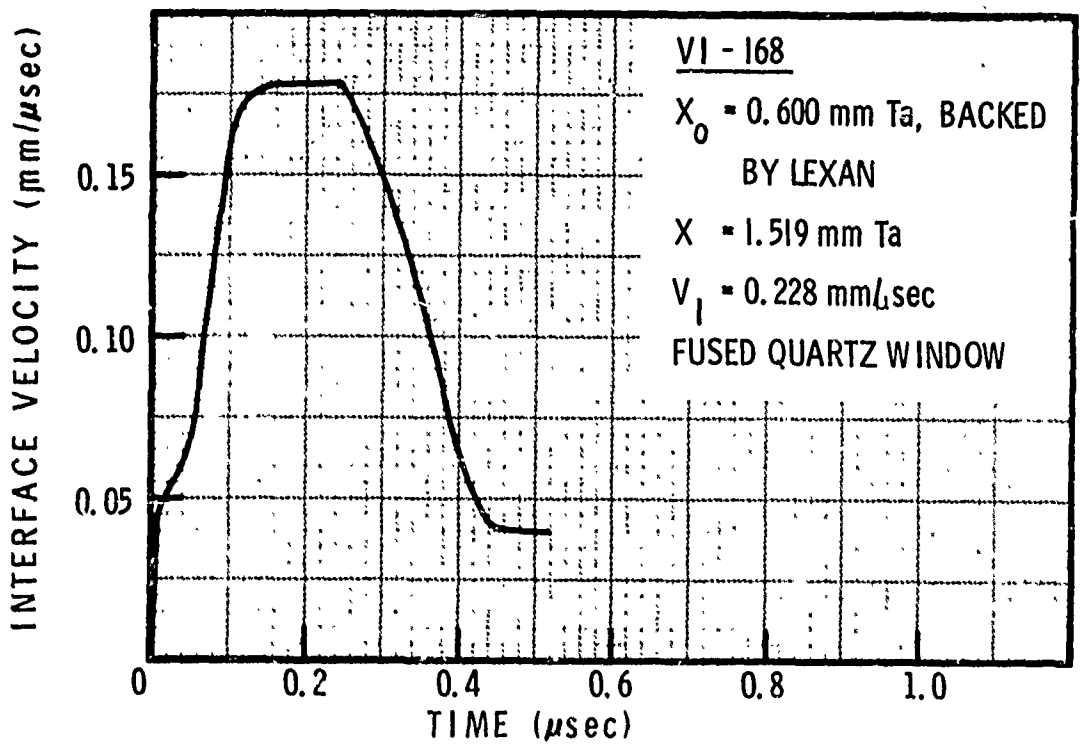
VI - 168
X_0 = 0.600 mm Ta, BACKED BY LEXAN
X = 1.519 mm Ta
V_I = 0.228 mm/μsec
FUSED QUARTZ WINDOW
INTERFACE VELOCITY (mm/μsec)
0.15
0.10
0.05
0
0.2
0.4
0.6
0.8
1.0
TIME (μsec)

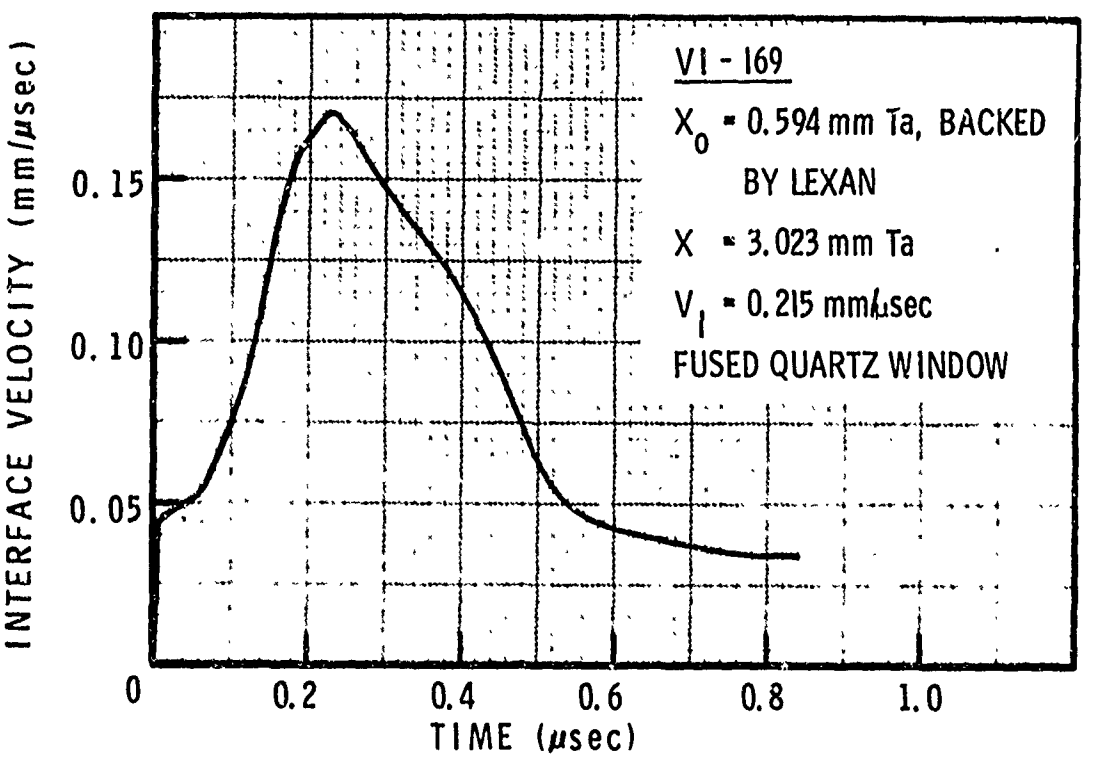
VI - 169
X_0 = 0.594 mm Ta, BACKED BY LEXAN
X = 3.023 mm Ta
V_I = 0.215 mm/μsec
FUSED QUARTZ WINDOW
INTERFACE VELOCITY (mm/μsec)
0.15
0.10
0.05
0
0.2
0.4
0.6
0.8
1.0
TIME (μsec)

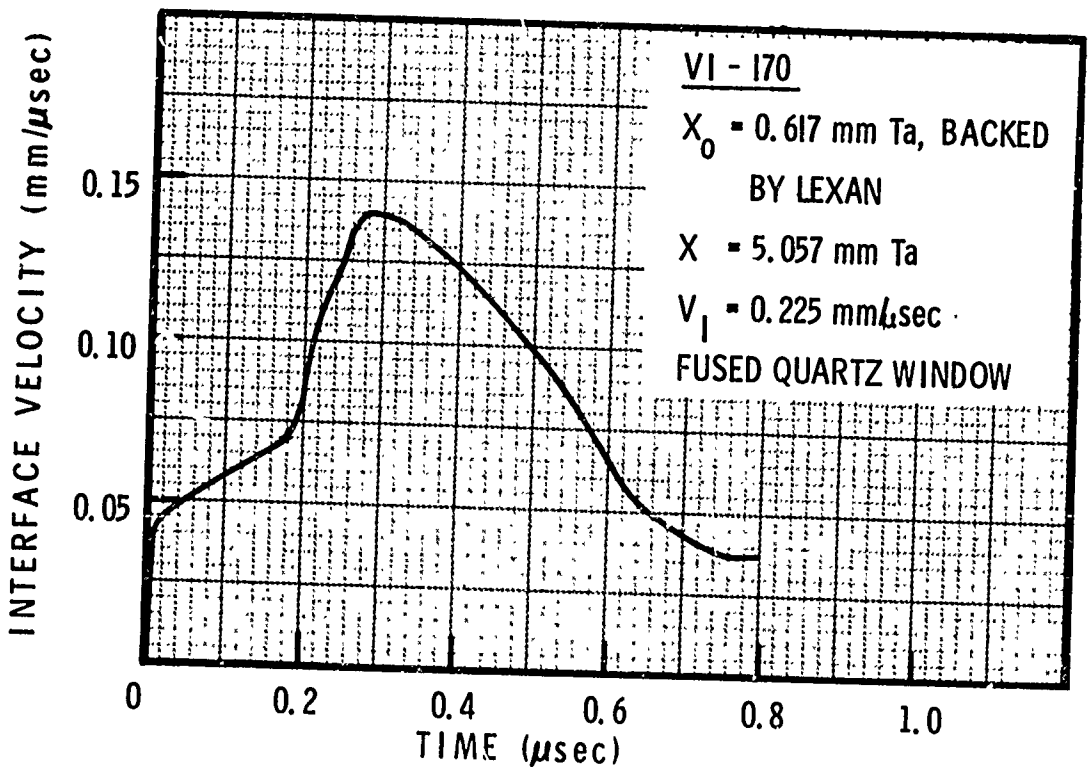
VI - 170
X_0 = 0.617 mm Ta, BACKED BY LEXAN
X = 5.057 mm Ta
V_I = 0.225 mm/μsec
FUSED QUARTZ WINDOW
INTERFACE VELOCITY (mm/μsec)
0.15
0.10
0.05
0
0.2
0.4
0.6
0.8
1.0
TIME (μsec)

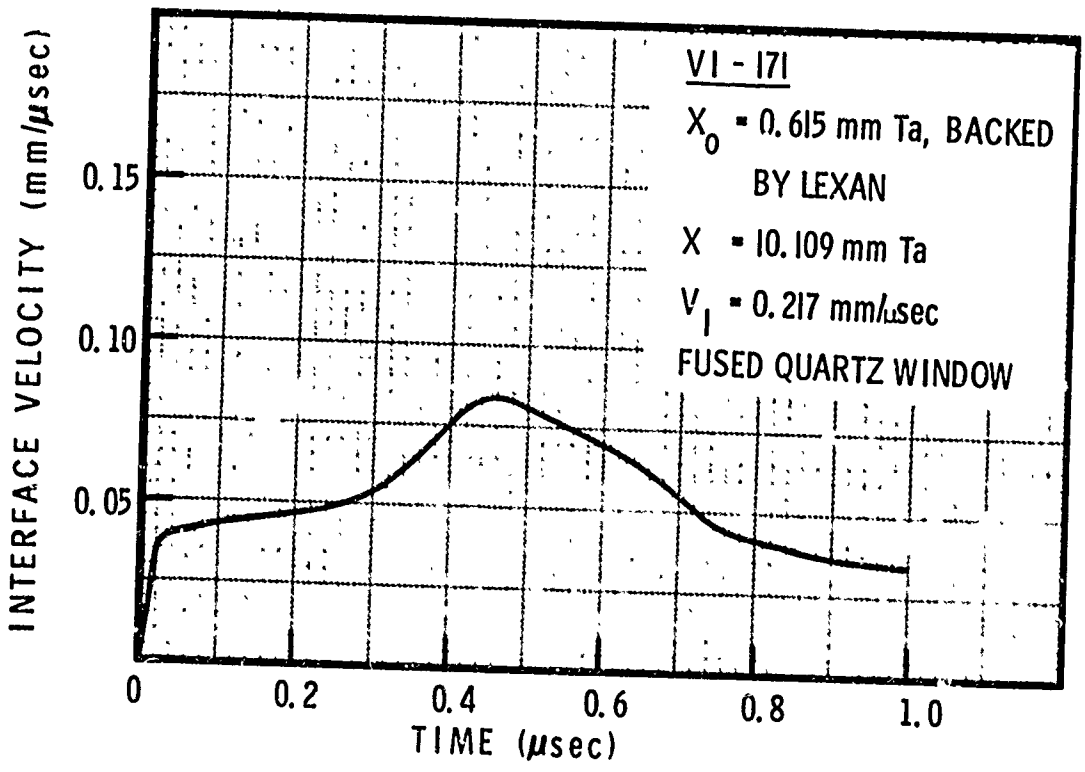
VI - 171
X_0 = 0.615 mm Ta, BACKED BY LEXAN
X = 10.109 mm Ta
V_I = 0.217 mm/μsec
FUSED QUARTZ WINDOW
INTERFACE VELOCITY (mm/μsec)
0.15
0.10
0.05
0
0.2
0.4
0.6
0.8
1.0
TIME (μsec)

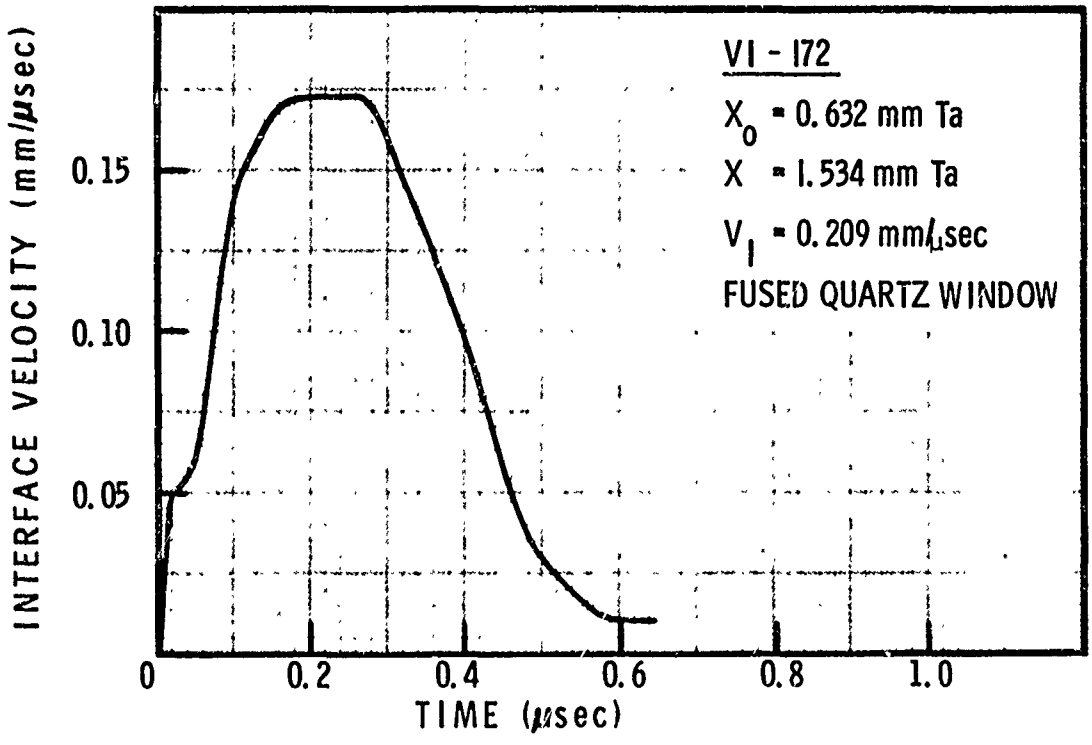
VI - 172
X_0 = 0.632 mm Ta
X = 1.534 mm Ta
V_1 = 0.209 mm/μsec
FUSED QUARTZ WINDOW
INTERFACE VELOCITY (mm/μsec)
0.15
0.10
0.05
0
0.2
0.4
0.6
0.8
1.0
TIME (μsec)

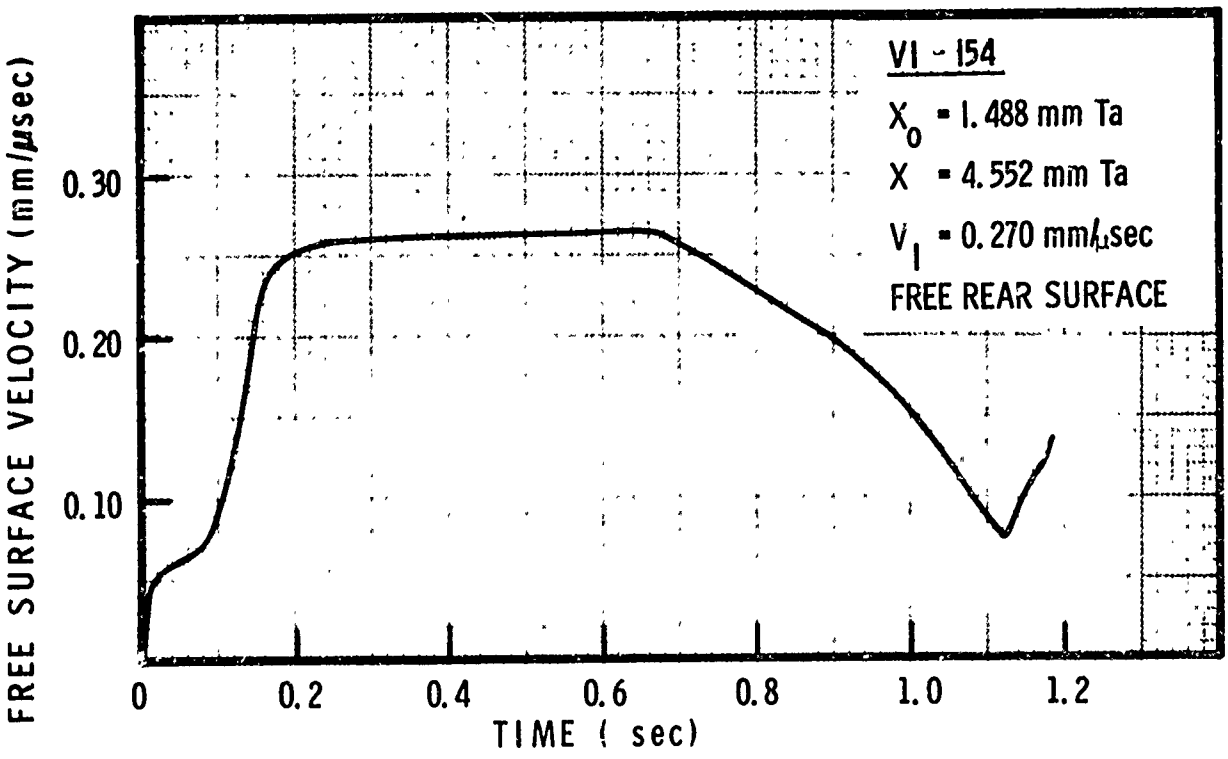
VI - 154
X_0 = 1.488 mm Ta
X = 4.552 mm Ta
V_1 = 0.270 mm/μsec
FREE REAR SURFACE
FREE SURFACE VELOCITY (mm/μsec)
0.30
0.20
0.10
0
0.2
0.4
0.6
0.8
1.0
1.2
TIME (sec)

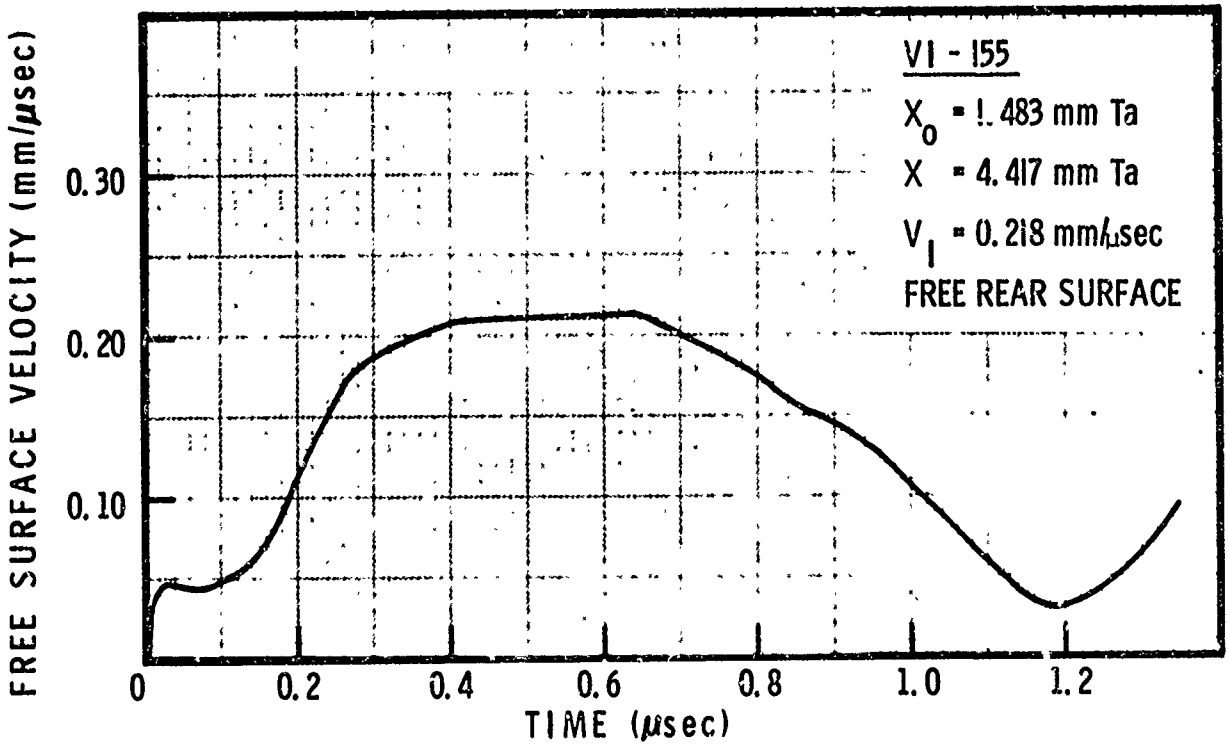
VI - 155
X_0 = 1.483 mm Ta
X = 4.417 mm Ta
V_1 = 0.218 mm/μsec
FREE REAR SURFACE
FREE SURFACE VELOCITY (mm/μsec)
0.30
0.20
0.10
0
0.2
0.4
0.6
0.8
1.0
1.2
TIME (μsec)

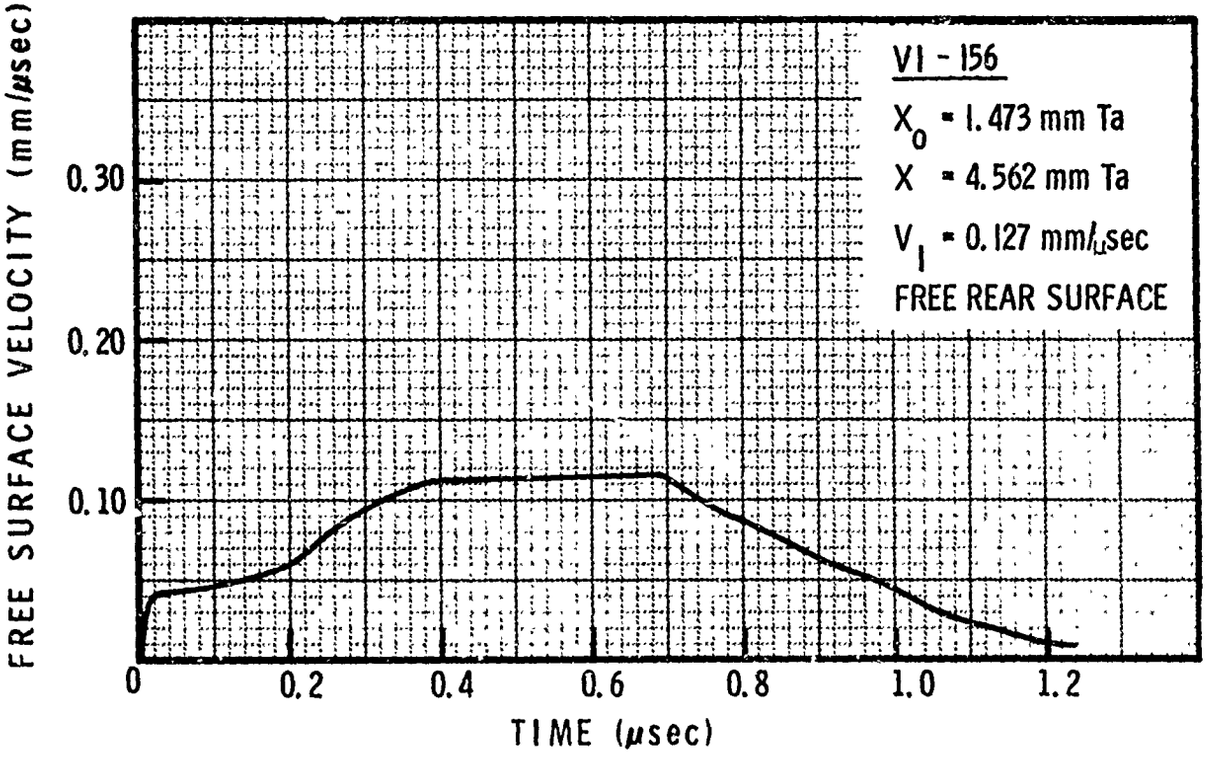
VI - 156
X_0 = 1.473 mm Ta
X = 4.562 mm Ta
V_1 = 0.127 mm/μsec
FREE REAR SURFACE
FREE SURFACE VELOCITY (mm/μsec)
0.30
0.20
0.10
0
0.2
0.4
0.6
0.8
1.0
1.2
TIME (μsec)

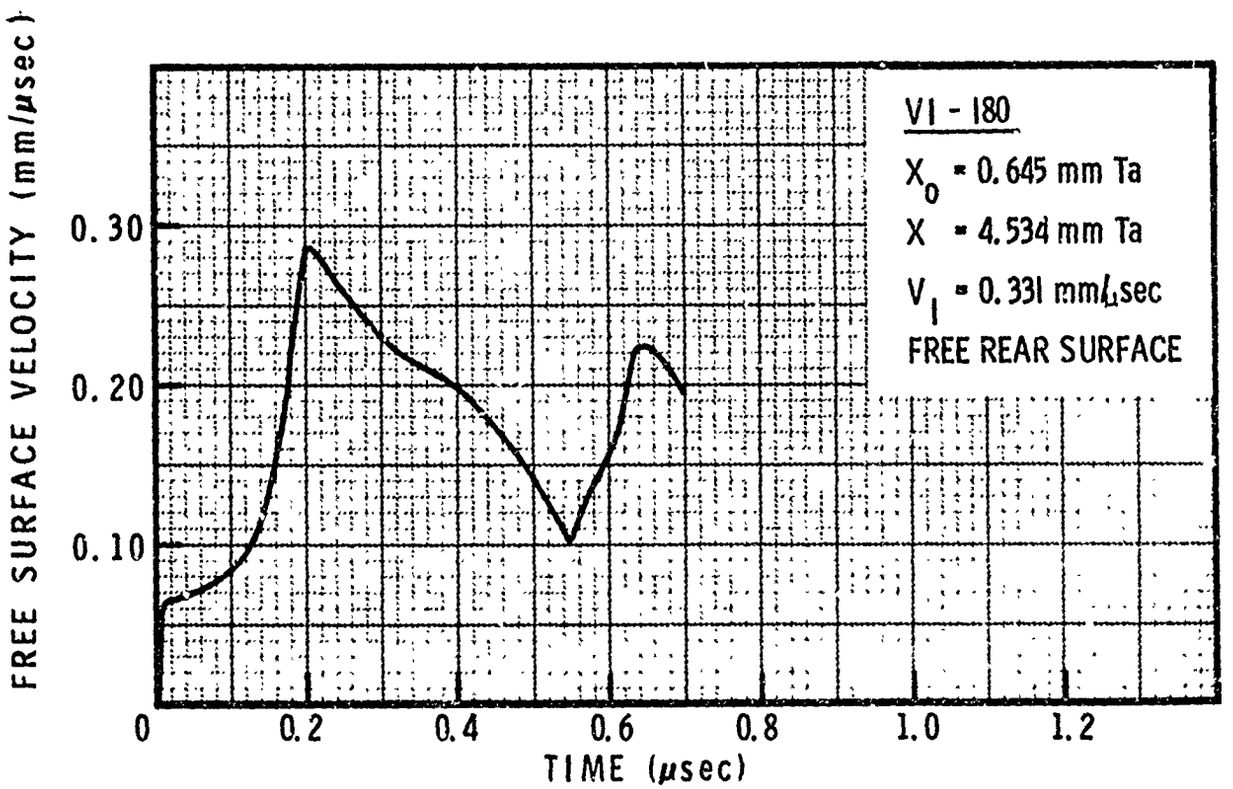
VI - 180
X_0 = 0.645 mm Ta
X = 4.534 mm Ta
V_1 = 0.331 mm/μsec
FREE REAR SURFACE
FREE SURFACE VELOCITY (mm/μsec)
0.30
0.20
0.10
0
0.2
0.4
0.6
0.8
1.0
1.2
TIME (μsec)

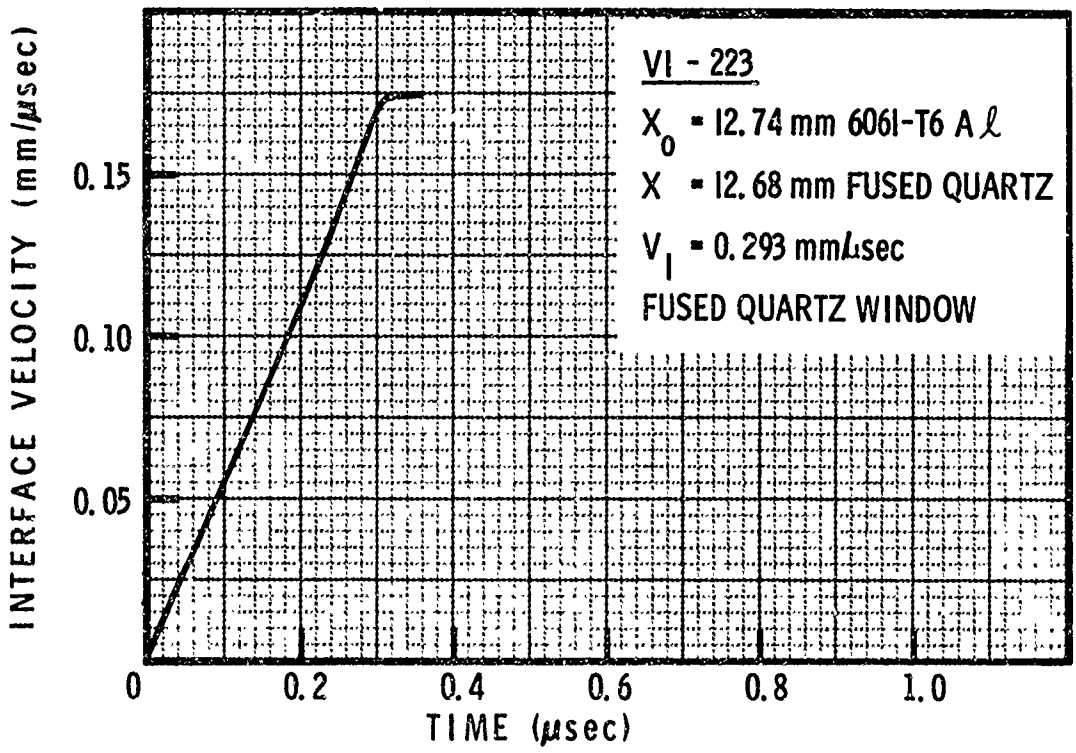
VI - 223
X_0 = 12.74 mm 6061-T6 Aℓ
X = 12.68 mm FUSED QUARTZ
V_I = 0.293 mm/μsec
FUSED QUARTZ WINDOW
INTERFACE VELOCITY (mm/μsec)
0.15
0.10
0.05
0
0.2
0.4
0.6
0.8
1.0
TIME (μsec)

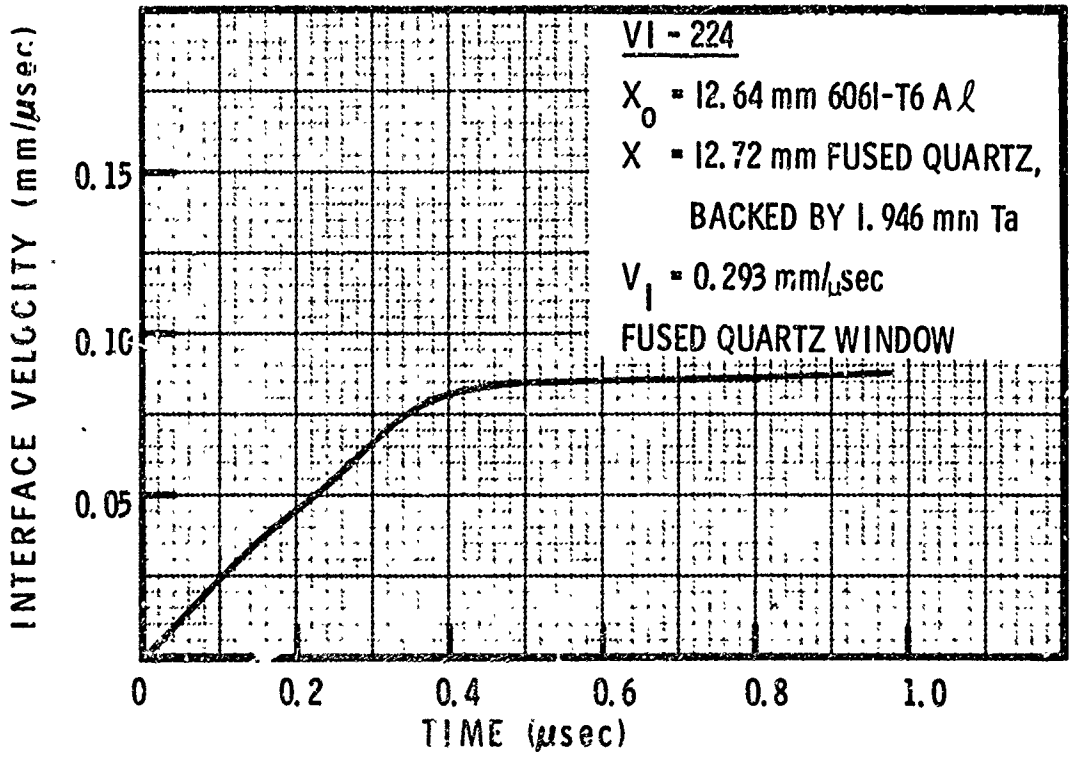
VI - 224
X_0 = 12.64 mm 6061-T6 Aℓ
X = 12.72 mm FUSED QUARTZ,
BACKED BY 1.946 mm Ta
V_I = 0.293 mm/μsec
FUSED QUARTZ WINDOW
INTERFACE VELOCITY (mm/μsec)
0.15
0.10
0.05
0
0.2
0.4
0.6
0.8
1.0
TIME (μsec)

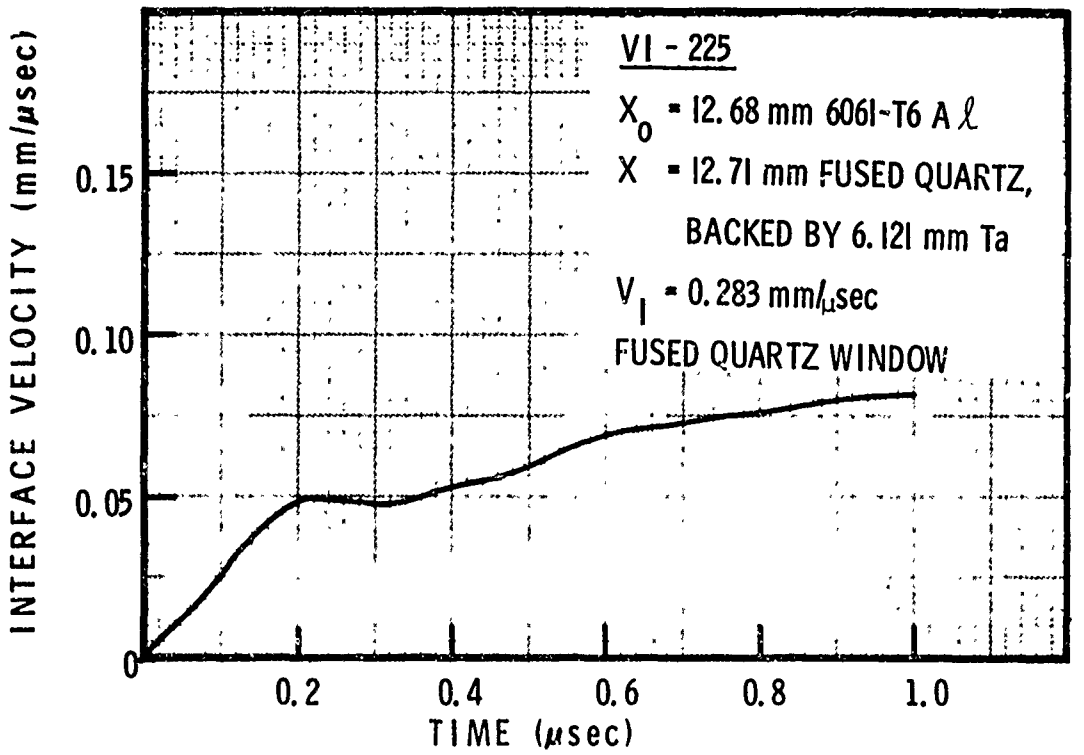
VI - 225
X_0 = 12.68 mm 6061-T6 A ℓ
X = 12.71 mm FUSED QUARTZ,
BACKED BY 6.121 mm Ta
V_I = 0.283 mm/μsec
FUSED QUARTZ WINDOW
INTERFACE VELOCITY (mm/μsec)
0.15
0.10
0.05
0
0.2
0.4
0.6
0.8
1.0
TIME (μsec)

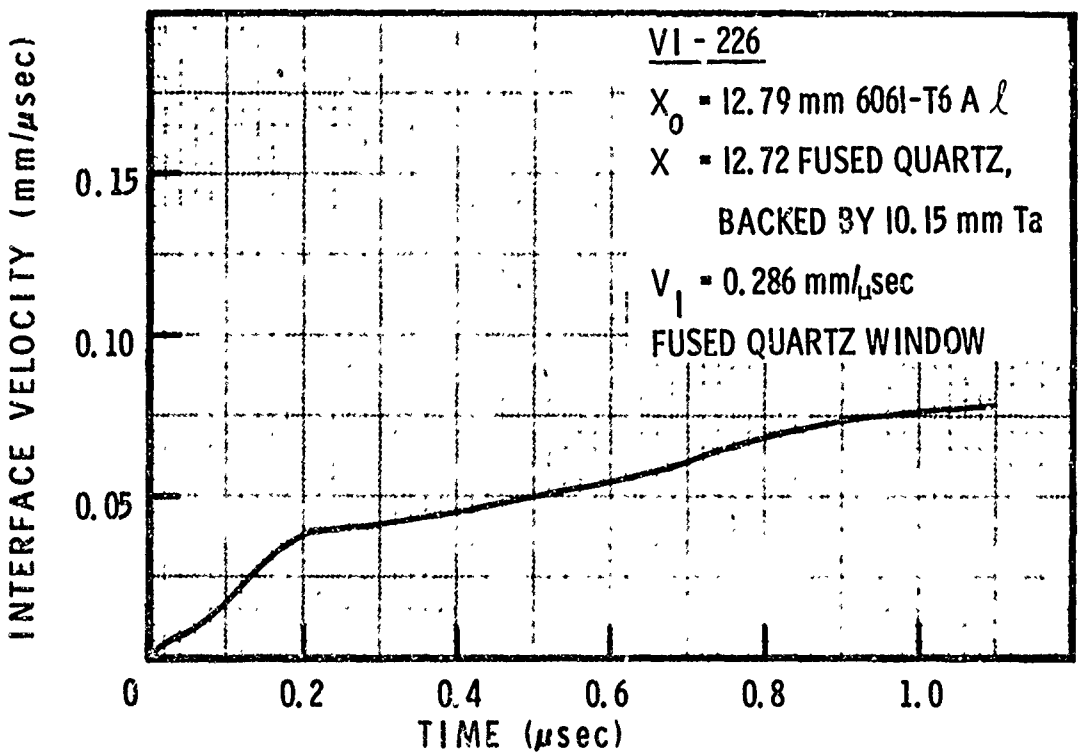
VI - 226
X_0 = 12.79 mm 6061-T6 A ℓ
X = 12.72 FUSED QUARTZ,
BACKED BY 10.15 mm Ta
V_I = 0.286 mm/μsec
FUSED QUARTZ WINDOW
INTERFACE VELOCITY (mm/μsec)
0.15
0.10
0.05
0
0.2
0.4
0.6
0.8
1.0
TIME (μsec)